








Article

Blue carbon cycling in the coastal areas of Qatar

Ivan Strakhov^{1,2} , Hadil Elsayed³ , Zach A. DiLoreto¹, Khoren Avetisyan¹, Zulfa Ali Al Disi³ , Khaled Naja³,
Hamad A. S. Al-Kuwari³ , Fadhil N. Sadooni³, Jassim Alkhatat³ and Maria Dittrich^{1,2,3} 

¹Biogeochemistry Group, Department of Physical and Environmental Sciences, University of Toronto Scarborough, 1065 Military Trail, Toronto, Ontario, M1C 1A1, Canada; ²Department of Earth Sciences, University of Toronto, 22 Ursula Franklin St., Toronto, Ontario, M5S 3B1, Canada and ³Environmental Science Center, Qatar University, P.O. Box 2713, Doha, Qatar

Abstract

Coastal wetland sediments are vital to the global carbon cycle as they represent large sinks of blue carbon – carbon from atmospheric and oceanic sources – which are threatened by ecosystem loss. The forms of sequestered carbon and the sequestration capability are affected by many bio- and geochemical factors that change unpredictably along coastal locales. In the present study, we investigated three unique coastal sites – a coastal mangrove and two sabkhas with contrasting geology and tidal influence in the Qatar peninsula – for their carbon capture ability to determine how biogeochemical indices affect their blue carbon sequestration potential. We applied a suite of biological and geochemical tools, collecting the sediment cores of approximately 40 cm depth; analysed sediment porewater; performed depth-profiling of the organic matter, sedimentary minerals, microbial community and analysis of sediment surface for pH, oxygen (O₂); redox potential and hydrogen sulfide (H₂S) by microsensors. High-resolution transmission electron microscopy with energy-dispersive X-ray spectroscopy (TEM-EDXS) and scanning transmission X-ray microscopy (STXM) revealed templating effects that promoted Mg-carbonate nucleation in coastal hypersaline environments. Microsensing reveals the intricacy of the oxic/anoxic transition at the sediment surface. Microbial DNA sequencing at various sediment depths shows the occurrence of microbial genera, whose functions explain the geochemical trends and carbon sequestration pathways observed at each site. Notably, we found that carbon sequestration in the mangrove and carbonate-sand sabkha was correlated with organic matter degradation and inorganic carbon content, while in the siliciclastic sabkha it was solely influenced by sediment density and depth.

Keywords: blue carbon; sabkha; coastal ecosystem; carbon sequestration; mangroves; hypersaline environment; tidal salt marches; carbonate

(Received 21 April 2024; revised 07 September 2024; manuscript accepted: 22 October 2024)

Introduction

Modern climate change, such as global warming, arising from anthropogenic impacts such as rising industrial carbon emissions, increasingly puts pressure on the global carbon cycle to sequester large amounts of carbon. Marine waters become acidified as atmospheric carbon dioxide (CO₂) is absorbed into the water, having detrimental impacts on marine organisms that use carbonate minerals in their shells. Marine coastal zones, such as sabkhas (intertidal hypersaline flats), mangroves and saline lake inlets, are major blue carbon sinks, enabling carbon storage with significant climatological implications (Eid *et al.*, 2022). The carbon sequestration abilities and mechanisms of marine coastal environments, which act as gates between terrestrial and oceanic systems, are governed by an array of different physical, geochemical and ecological factors – including upwelling of dissolved carbon to sediment porewaters, mineralization of carbonate minerals and organic matter (OM) and

deposition by microorganisms in the sediment (Bauer *et al.*, 2013; LaRowe *et al.*, 2020). Assessing the above-contributing factors in different coastal marine environments is essential to understanding coastal carbon stock trends and mechanisms of sedimentary carbonate mineral formation. Carbonate minerals such as dolomite and aragonite are a major part of the sedimentary inorganic carbon fraction within the overall blue carbon pool. Their authigenic and biogeochemical mineralization routes are forms of long-term inorganic carbon sequestration in sediments. Carbonate rocks are of major industrial interest due to being reservoirs of oil and natural gas (Burchette, 2012). Composing a significant portion of sedimentary rocks, carbonates are also used as a marker for early diagenesis at the Earth's surface (Areias *et al.*, 2022). The ability for carbon to be sequestered as carbonate minerals within coastal systems is thus relevant for industrial, conservation and geochronological studies.

The arid, evaporative and degradative conditions of near-shore sediments make coastal environments an effective organic and inorganic carbon sequestration system (Schile *et al.*, 2017). Geochemical and biological degradative processes favour the accumulation of organic and inorganic carbon compounds in the sediments. Organic carbon enters marine coastal sediments through various pathways,

Corresponding author: Maria B. Dittrich; m.dittrich@utoronto.ca

Cite this article: Strakhov I, Elsayed H, DiLoreto Z.A., Avetisyan K, Al Disi Z.A., Naja K, Al-Kuwari H.A.S., Sadooni F.N., Alkhatat J, & Dittrich M. (2025). Blue carbon cycling in the coastal areas of Qatar. *Geo-Bio Interfaces* 2, e3, 1–16.
<https://doi.org/10.1180/gbi.2024.8>

such as allochthonous tidal particulate deposition, upwelling of bioturbated benthic sediments and burial of microbial OM (LaRowe *et al.*, 2020). Inorganic carbon in marine sediments is sourced from dissolved CO₂ in interstitial water and carbonate ions from calcite dissolution or microbial productivity. Microbial communities within the sedimentary stratigraphic column act in concert to cycle carbon as organic carbon by synthesizing extracellular polymeric substances (EPS), which can template carbonate formation. Cyanobacteria in microbial mats, have been shown to re-use EPS to further cycle organic carbon (Stuart *et al.*, 2016). Coastal near-surface microbiota at the sediment–water interface (SWI), such as anoxygenic phototrophs and sulfide-oxidizing bacteria (SOB), contribute to the fixing of inorganic carbon sources as organic EPS (Dupraz and Visscher, 2005). Deeper below the sediment surface, carbonates can be degraded and release component-bound ions (HCO₃⁻, Ca²⁺, Mg²⁺). On the other hand, microbial activity leads to increased alkalinity, promoting the authigenic formation of carbonate minerals such as dolomite (Dupraz and Visscher, 2005; Van Lith *et al.*, 2003; Wright and Wacey, 2005). Calcium (Ca²⁺) and magnesium (Mg²⁺) cations of sedimentary carbonate minerals are captured from upwelled surface waters by binding to the negatively charged microbial cell surface and EPS. EPS have a ‘templating’ effect on dolomite and high-Mg calcite formation by de-hydration of Mg²⁺ cations, stabilizing them for carbonate nucleation (Bontognali *et al.*, 2014; d’Abzac *et al.*, 2013; Paulo *et al.*, 2020; Perri *et al.*, 2018). The combined effect of coastal sediment geochemistry and microbial community metabolism influences the fate of organic and inorganic fractions of blue carbon as it undergoes the cycle of deposition, EPS conversion, burial, microbial degradation and carbonate re-mineralization. However, whether coastal site-specific carbon biogeochemistry affects the carbon sequestration ability and primary mechanism needs clarification.

The Qatar peninsula presents an opportunity to study coastal sites with unique biogeochemical characteristics to distinguish the carbon sequestration dynamics. OM degradation is the central factor that links organic carbon cycling, inorganic carbonate mineralization and microbial activity in warm, hypersaline sediments (Burns *et al.*, 2000; DiLoreto *et al.*, 2021; Rivers, 2023). However, to date, there has been minimal inquiry into the connection between carbon sequestration, OM degradation and microbial activity in Qatari coastal sediments. Two Qatari coastal intertidal flats hosting microbial mats at the SWI showed significantly different carbon stocks and organic carbon burial profiles (Al Disi *et al.*, 2023). Redox conditions, pH and carbonate mineral saturation in a Qatari coastal microbial mat were attributed to OM and EPS degradation (Perri *et al.*, 2018), but the OM contribution was never quantified. Mangrove sediments were found to effectively re-mineralize degraded or disturbed organic matter (Santos-Andrade *et al.*, 2021), but the study of microbial activity and porewater chemistry is necessary to clarify the mechanisms of carbon cycling. The carbon–nitrogen (C:N) ratio has been used as an effective marker of sedimentary organic matter (SOM) degradation rate (Leifeld *et al.*, 2020) as it represents a progressive alteration of labile organic C sources (high N) to stable inorganic C-bearing minerals (high C). As noted before, the mineralization of carbonate minerals depends on the degradation state of the OM. C:N analysis is thus of importance to the study of sedimentary carbon sequestration where OM nutrient availability for microbial metabolism is a major factor limiting the sequestration of blue carbon.

In the present study, we aimed to combine and compare several geochemical and biological indicators of carbon sequestration in a variety of evaporitic hypersaline coastal ecosystems, to the magnitude

of blue carbon stored there and to the occurrence of sedimentary carbonates such as dolomite. An analysis of depth profiles of dissolved substances at the sediment–water interface (SWI) at high spatial resolution together with sedimentary microbial community analyses enabled the comparison of carbon cycling pathways and the sequestration potential in the studied environments. The result is a thorough assessment of the inorganic and organic carbon sequestration capability of Qatari coastal sediments.

Methods

Field sampling, site description and microsensor analysis

Field sampling of three study sites was performed during December 2021 and October 2022. Khor Al Adaid Sabkha (KAAS), at the southeast end of Qatar, is a national reserve region with aeolian sand dunes and a prominent inland sea. On the west side, there is an isolated pond (KAAS Salt Pond site, Fig. 1) with pink microbial mats which are covered in precipitated salts (Fig. 2a). The sediment in KAAS is primarily consisting of quartz with aragonite (DiLoreto *et al.*, 2019). Dohat Faishakh (DF site, Fig. 1) is a coastal sabkha on the west of Qatar with long stretches of shallow waters inhabited by green microbial mats (Fig. 2b). Above the intertidal zone, there are dry, evaporitic sediments rich in gypsum lenses. Dohat Faishakh has been described previously as hosting buried microbial mats along with dolomite in the sub-surface sediment (Brauchli *et al.*, 2016; Petrash *et al.*, 2017). The mangroves near Al Khor on the northeast shore of Qatar (AK site, Fig. 1) are fed by upwelled tidal streams and hold stagnant waters above muddy, bioturbated sediments (Fig. 2c). Acrylic tubes of 4 cm diameter and 45 cm length were used to obtain sediment cores at each of the sites. Tubes were cut in half lengthwise, secured with waterproof tape and split open in a sterile lab to obtain samples for all geochemical measurements and biological sequencing. Fractions of sediment layers were freeze-dried and powdered to <5 µm particle size with a Retsch steel ball mill. All geochemical analyses were reported per gram of dry weight (DW) of sediment.

Oxygen, pH, redox and sulfide microsensors (Unisense) were calibrated before each field sampling by the following methods. Amperometric O₂ and H₂S microsensors were pre-polarized in de-ionized water. Oxygen microsensors were two-point calibrated in O₂-saturated water and reduced water by air-bubbler apparatus and sodium hydrosulfite suspension respectively. The pH microsensor was calibrated by pH 4, 7 and 10 buffer solutions. The redox microsensor was two-point calibrated using quinhydrone-saturated pH 4 and 7 buffers. The sulfide microsensor was two-point calibrated with 1 mM Na₂S and pH 1 buffer as the zero-point. The microsensors were mounted in the field on a millimetre-graded microsensor stand and connected through a 4-channel digital multi-meter to a laptop with Unisense Logger software. The microsensors were moved down in 0.5–2 mm increments until 2 cm below the SWI, where larger resolution readings were obtained.

Total carbon and nitrogen and total organic carbon analysis

Core layer samples of 0.2 g of freeze-dried sediment were loaded into small tinfoil trays (LECO), which were twisted shut. Total carbon (TC) and total nitrogen (TN) were analysed with a LECO CN628 series analyser. The instrument was baselined first with 7–8 blank burn cycles until the C and N values obtained were stable, indicating that the instrument was flushed. The instrument was calibrated for the analysis with three aliquots of 0.15 g of EDTA.



Figure 1. Locations of study sites. Red pins indicate where microsensors were performed and sediment core samples were extracted: (a) Map of Qatar showing an overview of the primary study locations; (b) Dohat Faishakh (DF) Sabkha, located on the northwestern coast; (c) Al Khor (AK) Mangroves site overview; (d) Khor Al Adaid Sabkha Salt Pond (KAAS Salt Pond) site, on the west side of the inland sea on the south of Qatar.

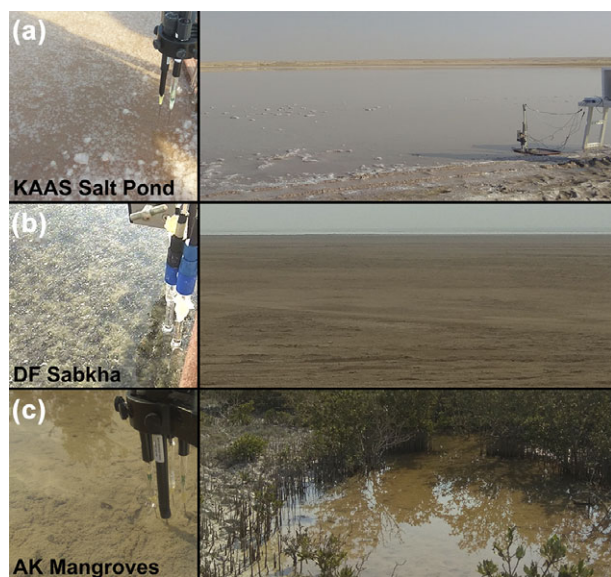


Figure 2. Field study site images with insets (left) showing the sediment–water interface: (a) Khor Al Adaid Sabkha (KAAS) Salt Pond; (b) Dohat Faishakh (DF) Sabkha; (c) Al Khor (AK) Mangroves.

Total organic carbon (TOC) was determined with a solids TOC attachment for the Shimadzu TOC-L spectrophotometer, which measures the total inorganic carbon fraction evolved as CO_2 from reaction with phosphoric acid and subtracts it from the total carbon measurement.

Total phosphorus analysis

Fractions for total phosphorus (TP) were extracted from the sediment by digestion with potassium persulfate and 0.5 N sulfuric acid

in a 2-hour autoclave cycle (Patton and Kryskalla, 2003). The digested samples were diluted and mixed with a colouring reagent consisting of ammonium molybdate, L-ascorbic acid and antimony potassium tartrate in sulfuric acid (EMSL, 1993). After thirty minutes of colour development, the absorption was measured by UV-visible spectrophotometry at 883 nm and the TP concentration was calculated from a phosphate standard (RICCA) curve.

Chlorophyll analysis

Chlorophyll was extracted from wet sediment placed in aluminium foil-wrapped glass test tubes by repeated freeze/thaw and sonication cycles of approximately 5 grams of sediment in 90% acetone, followed by 12-hour incubation at 4°C in the dark. The extracted solution was then measured on a plate reader absorption spectrophotometer at 470, 630, 647, 664, 665 and 750 nm to determine chlorophyll-*a*, -*b* and -*c* concentrations by the tri-chromatic method (Jeffrey and Humphrey, 1975).

X-ray diffractometry

X-ray diffraction was conducted using a Bruker D8 Advance diffractometer with a copper tube emission source and anti-air scatter screen. The operating parameters were 30 kV, 25 mA, 10–60°2θ range, 0.01° step size, 0.75 seconds per step and 10 stage rotations per minute. The acquired spectra were indexed against the International Centre for Diffraction Data (ICDD) database to determine the major mineral species present.

16S ribosomal RNA sequencing

Aliquots from the field sediment cores were sampled under sterile conditions and preserved in RNAlater® stabilization solution until analysis. Microbial DNA was extracted from the sabkha sediments using a Qiagen PowerSoil extraction kit (Qiagen, USA). The

extracted DNA was sequenced by MR DNA Laboratories (MR DNA, USA). The 16S rRNA gene V4 variable region PCR primers 341F/785R were used to amplify the DNA, which was then purified on Ampure XP beads. An Illumina MiSeq was used to sequence the DNA according to manufacturer guidelines. The forward and reverse sequences were joined, <150 base pair sequences and ambiguous base calls were removed and sequences were quality-filtered using error threshold 1.0. Sequences were de-noised and chimera sequences removed, resulting in zero-radius operational taxonomic units (ZOTUs), which were classified using a BLASTn database (NCBI, US). Phylum- and genus-level ZOTUs with >4% abundance were reported.

Bulk density and organic carbon stock

The bulk density of sediment core layers was calculated using the following relationship reported by (Avnimelech *et al.*, 2001) for bulk density of flooded sediments:

$$\text{Bulk density (g/cm}^3\text{)} = 1.776 - 0.363 \cdot \ln(\text{OC}) \quad (\text{Eq. 1})$$

Where OC is the organic carbon concentration in mg C/g dry sediment. Organic carbon stock (C_{org} stock) in the sediments was calculated using the following formula described in (Howard *et al.*, 2014):

$$\text{Bulk density (g/cm}^3\text{)} = 1.776 - 0.363 \cdot \ln(\text{OC}) \quad (\text{Eq. 2})$$

Scanning electron microscopy and energy-dispersive X-ray spectroscopy

Scanning electron microscopy was performed on a Hitachi SU-7000 SEM running at 10 kV in variable pressure mode using freeze-dried and fractured sediment from each site at a depth of 20 cm mounted to carbon tape. An Oxford Instruments energy-dispersive X-ray spectroscopy (EDXS) detector and Aztec analysis software were used to identify the elemental composition of mineral particles in the samples.

Porewater multi-element analysis

Porewater was extracted in the field by use of Rhizons (RhizonsTM) and preserved with the addition of 20 μL of 5% HNO_3 . Concentrations of trace elements in the porewater were analysed using a Thermo Scientific iCAP Pro ICP-OES spectrophotometer with a 100 $\mu\text{g/mL}$ multi-element standard (SCP Science), 5% HNO_3 blank and the porewater diluted 500x with 5% HNO_3 to pH less than 2.

Scanning transmission X-ray micro-spectroscopy

Scanning transmission X-ray micro-spectroscopy (STXM) was performed at the PolLux beamline at the Swiss Light Source at the Paul Scherrer Institut to obtain Ca and C chemical maps of the DF site sediment. The layer at 11 cm depth was chosen based on previously reported TOC% and dolomite occurrence at this depth (Brauchli *et al.*, 2016). Fresh sediment samples, minerals (calcite, aragonite and dolomite) and an organic standard (EPS extracted from green microbial mats located at Khor Al Adaid's sabkha) were suspended in MilliQ and deposited on silicon nitride windows (Norcada, Canada) with 100 nm window thickness and 1.0 x 1.0 mm window size. The target energy ranges were the C K-edge (285–295 eV) and the Ca $L_{2,3}$ -edge (345–355 eV) and associated near-edge X-ray absorption fine structures (NEXAFS) in the X-ray absorption spectrum. Instrument parameters for spectra were: 40 μm entrance slit, 10 μm horizontal and vertical exit slit, 2 s dwell

time and 700 spectral points. Parameters for spectral imaging were: 40 μm entrance slit, 25 μm horizontal and vertical exit slit, 30 ms dwell time and 700 spectral points. The chosen parameters ensured a <50 nm spatial resolution and a <0.1 eV energy resolution to resolve NEXAFS. Spectra and images were reconstructed in aXis2000 software, extracting spectra from multiple ROIs in a chemical map. The NEXAFS spectral features (*i.e.*, peak shifts, broadening, attenuation and auxiliary peaks) in the C K-edge and Ca $L_{2,3}$ -edge regions indicated chemical alterations of the C- and Ca-containing organic matter and minerals in the sediment sample.

Transmission electron microscopy and energy dispersive x-ray spectroscopy

Transmission electron microscopy (TEM) was performed on a Thermo Fisher Talos 200X operating at 80 kV at the Canadian Centre for Electron Microscopy. Fresh sediments from the DF site at 11 cm depth were prepared by drop suspension and drying at ambient temperature on copper TEM grids without a formvar membrane (carbon-free). Mineral particles were imaged with high-resolution bright-field imaging (HR-TEM). Selected-area electron diffraction (SAED) imaging of mineral particles was done with a 10 nm SAED aperture to determine the mineral identity. EDXS chemical mapping of Ca, Mg, C and O was performed with a Super-X detector, using 20 μs dwell time. Diffraction patterns were indexed in *ImageJ* to determine mineral particle identity. EDXS spectra were processed in Velox software to show elemental mapping and localization.

Principal Component Analysis Statistics

Principal Component Analysis (PCA) was performed by *OriginPro* (2021), assessing the depth, TOC, TIC, C:N, TP, chlorophyll and bulk density data from each site. Pearson correlation coefficients were tested to determine correlations between sediment characteristics with respect to depth and the other measured characteristics. Strong ($R^2 > 0.5$) and significant ($p < 0.05$) correlations between sediment characteristics were reported and summarized in Table S1.

Results

Geochemical conditions at the sediment–water interface

Microsensor profiles show the rapidly changing geochemical conditions going from the surface water down through the SWI and in the sub-surface sediment at each of the study sites (Fig. 3a-c). The overlaying water oxygen concentration of the sites was 65–85 μM at KAAS Salt Pond, 0.7–0.8 mM at DF and 0.35–0.4 mM at AK. The O_2 concentration at the SWI peaked at 0.140 mM at the KAAS Salt Pond, 1.33 mM at DF and 0.64 mM at AK before dropping to near zero below 0.3 mm depth at KAAS Salt Pond and DF, immediately below the SWI at AK. The redox potential profiles follow a similar trend as the O_2 profiles. The overlaying water had a positive redox potential of +200–250 mV, increasing slightly at the SWI, then rapidly going to around –300 mV in the next 0.5 cm below, with an exception in DF that decreases to –40 mV at 1.2 cm depth, then increasing to +123 mV at 3.9 cm depth.

The pH level rose at the SWI from 8.36 at DF and 8.63 at AK, after which the pH decreased rapidly toward the deeper layers to 7.10 at DF and 7.29 at AK, respectively. At the KAAS Salt Pond, the pH decreased steadily from 8.91, briefly stabilizing at 8.75 at the SWI and decreasing to 8.40 at 3 cm below the SWI. Sulfide concentration trends were variable across sites.

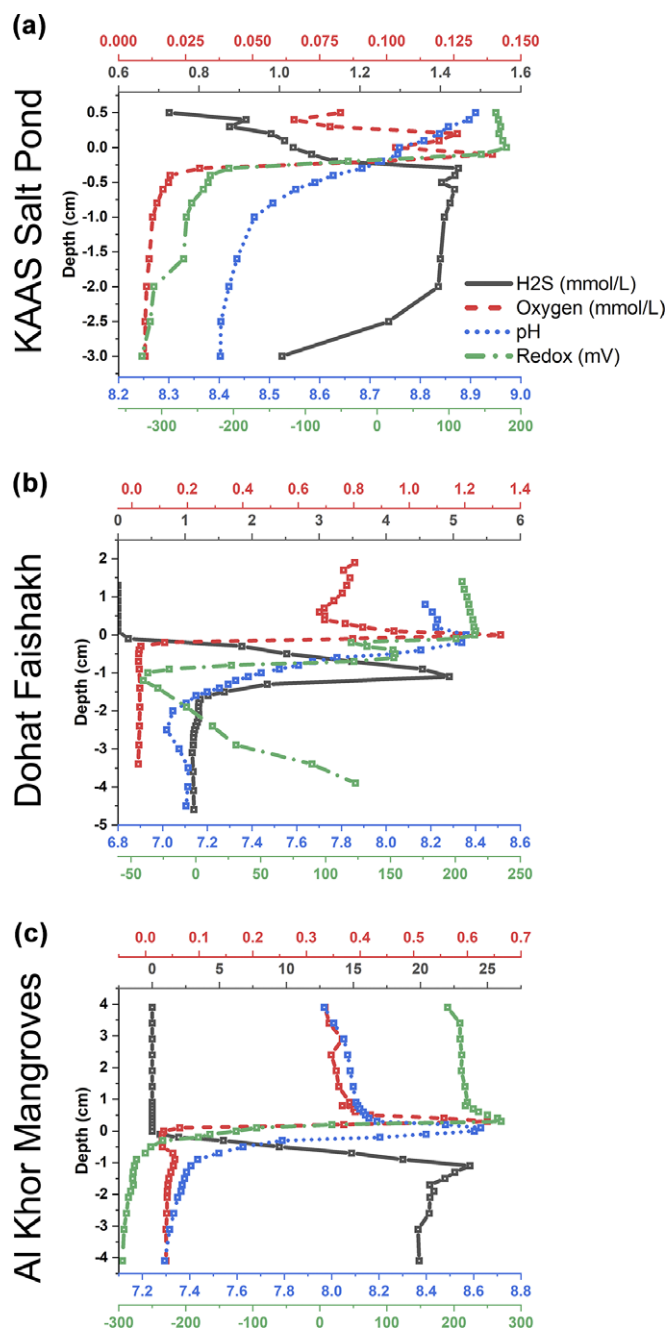


Figure 3. Microsensor depth profiles of the dissolved substances. KAAS and AK profiles were obtained in December 2021 and the DF profile was obtained in October 2022. Sulfide (solid black line), oxygen (dashed red line) concentrations, pH (dotted blue line) and redox potential (dash-dotted green line) at the SWI. The SWI is at depth 0.

Sulfide increased greatly below the SWI in the Al Khor mangroves, from zero in the surface water to a maximum of 23.7 mM, stabilizing at 19.9 mM at 3–4 cm below the SWI. At the KAAS Salt Pond, sulfide concentration began at 0.73 mM at the air-water interface and increased to a peak of 1.45 mM, just below the SWI and remained near this value for 2 cm below the SWI before decreasing in lower layers. At DF, sulfide concentration began to increase from zero at 0.1 cm below the SWI, peaking at 4.94 mM at 1.1 cm sediment depth, then decreasing and remaining around 1.10 mM at 1.6 cm below the SWI.

Thus, overlaying waters at all the sites are oxic and alkaline and the top 0.1 cm of the sediment at the SWI has significantly higher

oxygen concentration and a high redox potential. Below the SWI, the porewater quickly becomes anoxic. The redox potential falls to negative values, with the exception of DF where it increases again below 1 cm in depth. The pH approaches neutral values, except at KAAS Salt Pond where it remains alkaline. The sulfide concentration spikes and approaches lower values in the sub-surface depths.

Depth profiles of sediment characteristics: TOC, C:N, TP, chlorophyll, dissolved metals and mineralogical composition

KAAS salt pond

At KAAS Salt Pond, the highest TOC% is in the surface layer (1.73%) followed by 1.07% at 1.0 cm depth, then all layers below decrease in TOC in correlation with depth ($R^2=0.62$, $p<0.05$), with small fluctuations in TOC until the core bottom (0.16% TOC) (Fig. 4a). TIC also has a significant negative correlation with depth ($R^2=0.58$, $p<0.05$). The top 20 cm of the core has a C:N ratio varying from 25–45, while beyond this depth the C:N ratio decreases to less than 5, with a significant correlation to sediment depth ($R^2=0.58$, $p<0.05$). The surface layer sediment is the most concentrated in TP (125.9 g P/ μ g DW) and chlorophyll (100.3 ng/g DW). TP decreases similarly to TOC, correlating with depth ($R^2=0.51$, $p<0.05$). The chlorophyll concentration immediately becomes less than 1 ng/g DW below the surface, increasing briefly to 2.8 ng/g DW at 7 cm depth. TOC has a strong positive correlation with chlorophyll concentration ($R^2=0.61$, $p<0.05$). The XRD spectrum at the surface layer of KAAS Salt Pond shows signals corresponding to aragonite in the (111) peak at $26.3^\circ 2\theta$. It is masked by the strong (101) peak of quartz; however, the aragonite (021) and (221) peaks at 27.3 and $45.9^\circ 2\theta$, respectively, are detectable. These peaks maintain approximately the same intensity throughout the core. Quartz is the most abundant mineral in the 0.5 cm and 8 cm core depths, as seen from the intense (101) peak at $26.6^\circ 2\theta$; however, at 33 cm depth this peak is greatly attenuated and gypsum is found to be the abundant mineral. The peaks corresponding to the dolomite reflections (104) at $31.0^\circ 2\theta$, (113) at $41.0^\circ 2\theta$ are easily identifiable at this depth, as well as the aragonite (111) peak at $26.3^\circ 2\theta$ and (221) peak at $45.9^\circ 2\theta$. PCA (Figure S4A) shows that 80.3% of the variance in the KAAS sediment data is sufficiently described by the first two principal components (PCs), with TOC, TIC, TP and chlorophyll eigenvectors aligning positively with PC1 and C:N aligning negatively to PC2.

DF sabkha

The DF sabkha site (Fig. 4b) was characterized with a surface layer TOC% of 1.35%, decreasing in the next 3 cm to a minimum of 0.27%, then increasing again to 1.45% at 11 cm depth. The TOC% remained around 1.4% until 20 cm in depth, decreasing at 28 cm to 0.76% and increasing to a maximum of 1.71% at the core bottom. The C:N ratio followed the same pattern: elevated to 60–90 in layers with higher TOC% and decreased to 20–45 in layers with lower TOC%. TOC had a strong significant positive correlation to the C:N ratio ($R^2=0.72$, $p<0.05$) at the DF site. TP was around 150–220 μ g/g DW near the surface layers and decreased to around 100 μ g/g DW at 34 cm depth. The chlorophyll concentration was greatest at the surface with 18.3 ng/g DW, then 1 cm below the surface layer at 3.3 ng/g and <0.1 ng/g in the deeper layers of the core. The XRD analysis for the DF site shows an abundance of gypsum throughout the sedimentary column, with the intense (021) peak at $20.5^\circ 2\theta$, (020) peak at $11.6^\circ 2\theta$ and (041) peak at $29.1^\circ 2\theta$, which overlaps slightly with the detectable (104) peak of calcite at $29.5^\circ 2\theta$. At 11 cm and 34 cm depths, the (111) and (021) peaks, as well as the signature

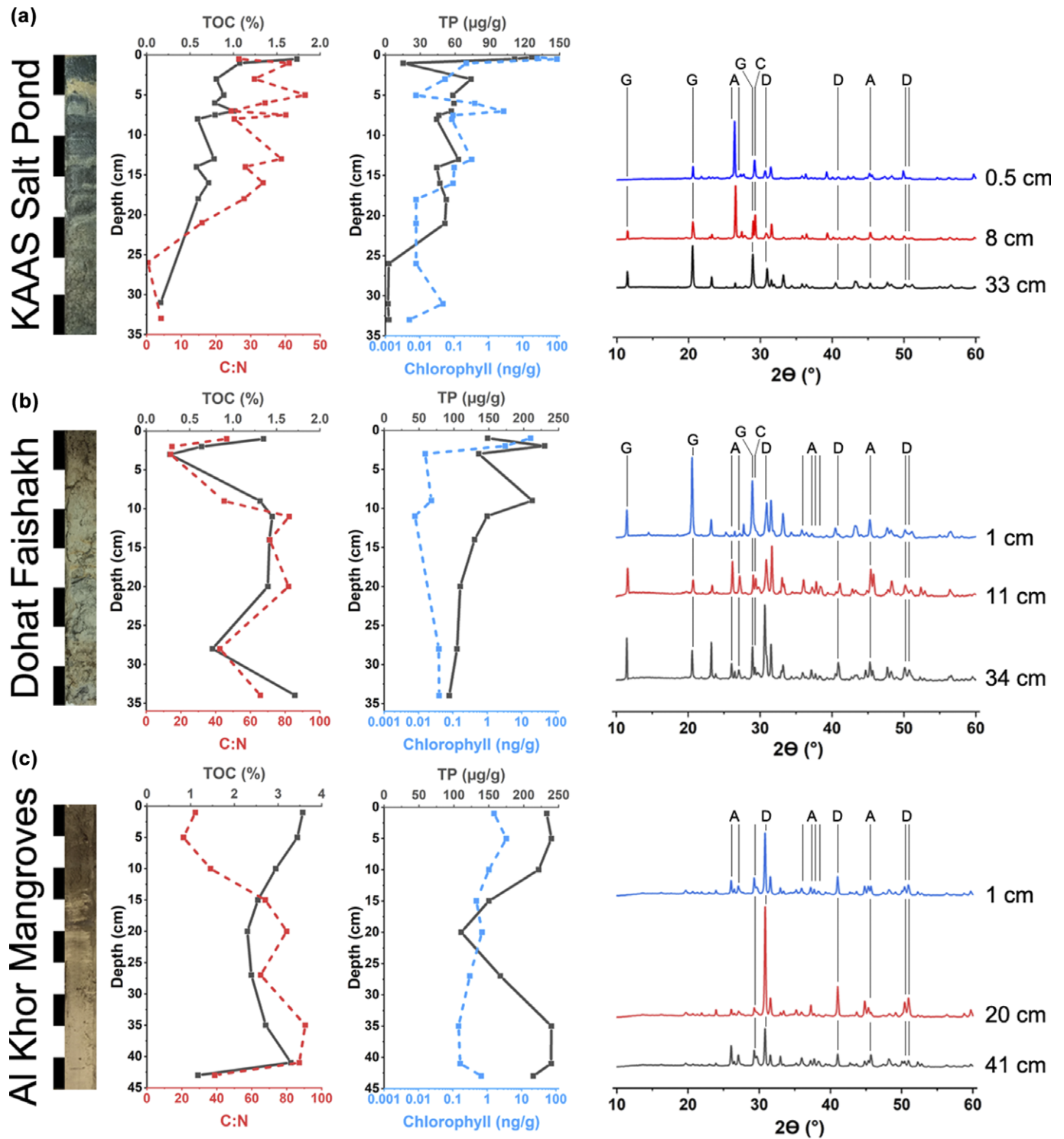


Figure 4. TOC, C:N ratio, TP and chlorophyll concentration sedimentary core profiles (left) with accompanying XRD spectra (right) of sedimentary layers in Qatari sabkhas. TOC profiles show high organic carbon content near the sedimentary surface layers and an increased C:N ratio in the layers directly below the surface, indicating high organic matter degradation rates. Chlorophyll concentrations are heightened at the sediment surface. TP profiles generally mirror the TOC profiles. XRD spectra show the mineralogy of selected layers in the sedimentary column, with lines indicating the most intense crystal reflections of aragonite (A), dolomite (D) and gypsum (G). Dolomite peaks are present and most intense in layers with high C:N signifying high OM degradation.

peaks of aragonite in the 36–39°2θ region, are prominent. Dolomite (104) and (113) peaks are also intense and well-resolved throughout all the studied depths at this site. The PCA biplot of the DF sediment data (Figure S4B) shows that two PCs describe 73.5% of the data variation. The TIC, TOC and C:N data are aligned with PC1 while TP and chlorophyll are strongly aligned to PC2.

AK mangroves

At AK (Fig. 4c), the surface TOC% was 3.57%. TOC decreased until 20 cm to 2.30%, steadily increasing again to 3.30% at 41 cm before falling to 1.17% at 43 cm at the core bottom. The C:N ratio at the surface of the core was 27.7 and, at a depth below 15 cm, the ratio spiked to higher values of between 60–90 before dropping down to

38.8 at 43 cm depth. The TP near the surface layers was 220–235 $\mu\text{g P/g DW}$, depleted near the middle 20 cm layer of the core at 110.4 $\mu\text{g P/g DW}$ and returning to $>200 \mu\text{g/g DW}$ below 35 cm depth. The level of chlorophyll was maximum in the top 10 cm of the core, between 1.1–3.6 ng chlorophyll/g DW and less than 0.71 ng/g DW in the deeper sediment. None of the measured sediment characteristics had significant relationships with sediment depth or other characteristics. The mineralogical composition of the AK sediment displayed no major peaks from either quartz or gypsum in the XRD spectrum. However, dolomite and aragonite characteristic peaks were very well-resolved and intense, with the most intense peaks for both minerals appearing in the 20 cm deep sedimentary layer. Of the variance in the AK sediment characteristic data, 72.5% is captured by the first two PCs in the PCA (Figure S4C). PC1 primarily describes negatively contributing TOC, TP and chlorophyll eigenvectors and positive bulk density depth eigenvectors. The main contributions to PC2 consist of negative contributing chlorophyll and bulk density and positive C:N eigenvectors.

Bulk density

Bulk density and C_{org} stock depth profiles for each site are reported in Figure S1. Bulk density at KAAS Salt Pond (Figure S1A) has a significant correlation with respect to depth ($R^2=0.80$, $p<0.001$), starting at 0.74 g/cm^3 at the layer just below the SWI and steadily increasing to 1.60 g/cm^3 at 32 cm depth. The C_{org} stock summed over the top 32 cm of sediment is 16.6 $\text{Mg C} \cdot \text{ha}^{-1}$. The bulk density of sediment at DF (Figure S1B) did not vary significantly with depth, fluctuating around 0.8–1.0 g/cm^3 throughout the core layers. The sum of C_{org} stock in the upper 35 cm of DF sediment was 31.3 $\text{Mg C} \cdot \text{ha}^{-1}$. Bulk density at the AK site (Figure S1C) did not vary with depth, remaining at 0.5–0.6 g/cm^3 throughout most of the core until 44 cm, where it rose to 0.88 g/cm^3 . The C_{org} stock sum in the top 35 cm of sediment was 19.0 $\text{Mg C} \cdot \text{ha}^{-1}$.

Porewater elemental analysis

Porewater analysis of the sites shows that Ca and Mg metals are abundant in the porewater. The Ca and Mg concentration of each site fluctuates in tandem with increasing depth (Figure S2). At KAAS Salt Pond (Figure S2A), Ca and Mg content in the surface layer was 990 ppm and 8935 ppm, respectively. At 1–3 cm below the SWI, Ca and Mg rise to 1491–1577 ppm and 11845–11375 ppm, respectively. At 6 cm depth, Ca and Mg fall to 101 ppm Ca and 2471 ppm Mg, rising at 7 cm to 2059 ppm Ca and 11793 ppm Mg. At 14 cm depth, both metals fall to 500 ppm Ca and 6822 ppm Mg and, at 31 cm, Ca is undetectable while Mg concentration is 1269 ppm. At the DF sabkha site (Figure S2B), Ca and Mg are absent in porewater until 9 cm depth with 2240 ppm Ca and 11520 ppm Mg. At 11 cm depth, both metals are slightly depleted to 766 ppm Ca and 7165 ppm Mg, rising again at 14–20 cm depth to 2401–2632 ppm Ca and 11576–11864 ppm Mg. At 34 cm depth, the metals fall to 566 ppm Ca and 7717 ppm Mg. At AK mangroves (Figure S2C), Ca and Mg concentrations remain around 1750–2110 ppm Ca and 5505–6505 ppm Mg with the maximum concentration of each occurring at 35 cm depth.

Micro-spectroscopy of sediment particles

SEM imaging of sediment from the Al Khor mangroves at 20 cm depth (Figure S3) reveals crystals with a distinct rhombohedral morphology. EDXS analysis of the crystals shows that their composition is primarily O (40.6 wt.%), Ca (26.0 wt.%), C (13.9 wt.%) and Mg (8.7 wt.%). Carbonates buried in the DF sediment can be

distinguished by their NEXAFS in the X-ray absorption spectra (Figure S5). Three ROIs in a DF sediment particle showed distinctly different NEXAFS signatures. The most distal region of the sediment particle (Figure S5B, blue dot) had a characteristic calcite identity, with the primary C K-edge peak of calcite matching the calcite standard at 290.1 eV and Ca $L_{2,3}$ -edge characteristic calcite a_1 , a_2 , b_1 and b_2 peaks at 349.0, 350.3, 352.4 and 353.7 eV, respectively. The lower-left region marked by the green dot consists mainly of organic matter as it exhibits the strong 288.5 eV C K-edge peak corresponding to carboxyl functional groups (Figure S5A), present also in the green EPS standard spectrum, and the absence of carbonate peaks in the Ca $L_{2,3}$ -edge region (Figure S5C). The region in the centre of the particle, marked by the red dot, possesses an identity closely resembling dolomite: the primary peak in the C K-edge region is characteristically right-shifted to 290.3 eV (Figure S5A), as well as shifts of the a_1 and a_2 Ca $L_{2,3}$ -edge carbonate peak positions to 349.2 and 350.4 eV, respectively (Figure S5C). The C K-edge spectrum of this ROI shows a strong absorbance at 288.5 eV, signifying abundant carboxyl functional groups in the OM of this ROI. HR-TEM imaging of the DF sediment at 11 cm depth shows polycrystalline mineral particles in the surrounding sediment matrix (Figure S6). Diffraction analysis using SAED shows diffraction rings from polycrystalline dolomite crystal plane reflections, namely the (104), (015) and (116) planes, which were also abundantly present in the XRD spectrum from the same DF sediment core layer (Fig. 4b), corresponding to 31.0, 37.4 and 51.0°2 θ , respectively. EDXS elemental mapping reveals that the particle is mainly composed of Ca, Mg, C and O (Figure S6, bottom).

Microbial community composition

Microbial DNA is prominent at the domain level, occupying $>90\%$ of the classified ZOTUs near the surface of the sedimentary columns, with archaeal DNA increasing in the bottom layers to around 20%, with the exception being in the KAAS Salt Pond site where archaea make up 43% of domain-level ZOTUs at 3 cm depth.

KAAS salt pond phyla

In the KAAS Salt Pond (Fig. 5a), *Proteobacteria* are the most abundant at the surface (42.1%), with the remainder made up of *Cyanobacteria* (17.4%), *Spirochaetes* (14.8%), *Bacteroidetes* (9.4%) and *Chloroflexi* (9.5%). At 4 cm depth, the *Proteobacteria* population falls (to 29.2%) while *Euryarchaeota* becomes the abundant phylum (41.1%), with the remaining composition comprised of *Bacteroidetes* (9.9%) and *Firmicutes* (10.5%). By 13.5 cm depth, proportions of *Proteobacteria* (8.8%), *Bacteroidetes* (9.9%) and *Euryarchaeota* (25.9%) become less prominent, while the proportion of *Firmicutes* increases (46.0%). A 19.5 cm depth marks the appearance of *Actinobacteria* (6.4%), with *Proteobacteria* and *Bacteroidetes* (8.5% and 10.3%, respectively) having similar measures as in the layer above, and *Firmicutes* making up just over half of the ZOTUs (50.6%).

DF sabkha phyla

In DF (Fig. 5b), the surface layer is made up of *Chloroflexi* (32.3%), *Proteobacteria* (24.0%), *Cyanobacteria* (21.3%), with smaller proportions of *Bacteroidetes* (7.1%), *Euryarchaeota* (4.9%) and *Firmicutes* (4.2%). At 4 cm depth, *Proteobacteria* remains the same (26.1%), while the population of *Bacteroidetes* (21.1%) and *Firmicutes* (16.6%) increases, *Chloroflexi* decreases (5.0%) and *Ignivibacteria* (7.2%) and *Actinobacteria* (15.9%) become prominent. At 12 cm in the sedimentary column, *Firmicutes* becomes the

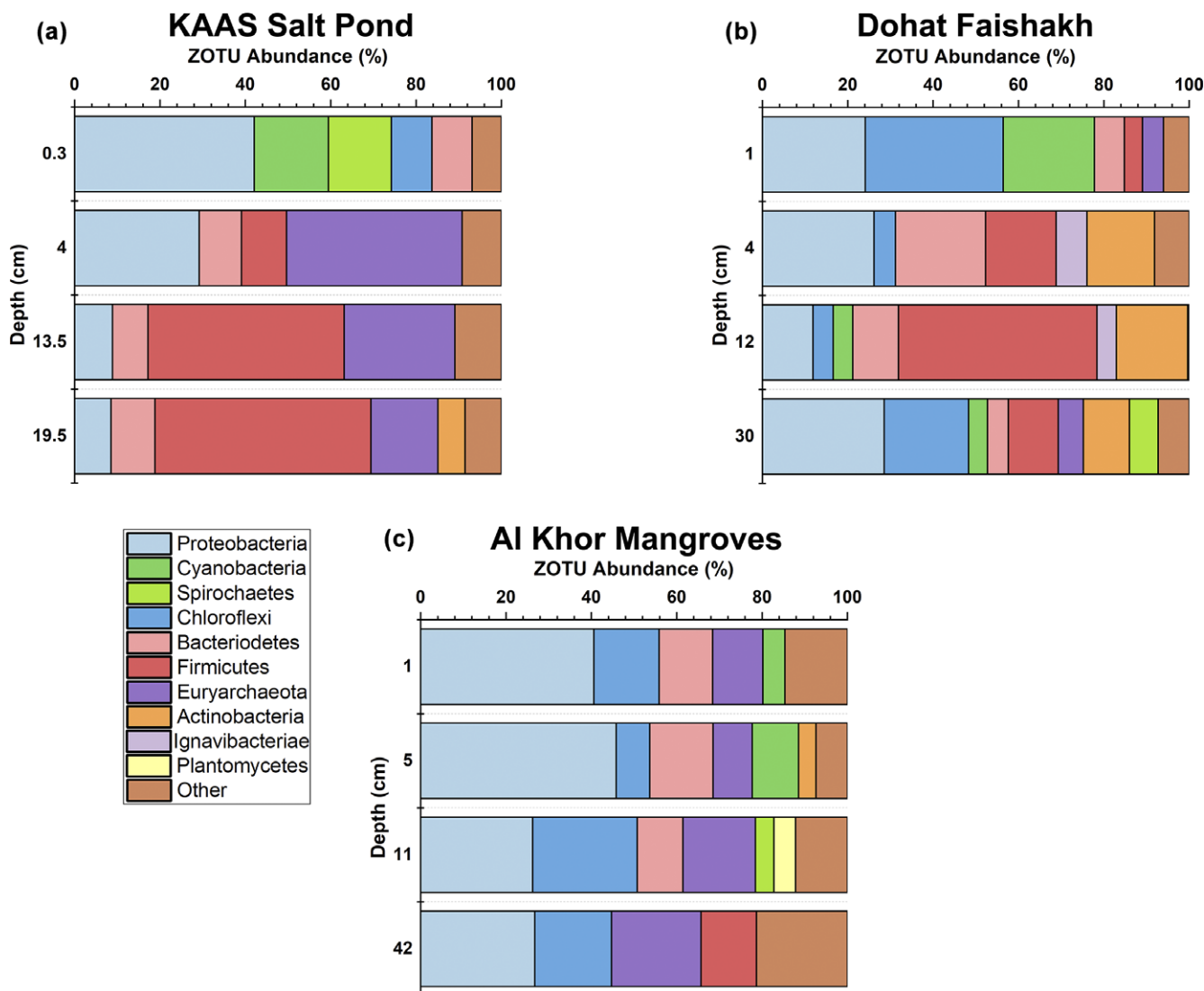


Figure 5. Phylum-level microbial community composition of the three sabkhas studied through column depth, as a percentage of ZOTUs: (a) Khor Al Adaid Salt Pond site; (b) Dohat Faishakh sabkha site; (c) Al Khor Mangroves site.

dominant phylum (46.5%), with the *Proteobacteria* (11.6%), *Chloroflexi* (4.7%), *Bacteroidetes* (10.7%) and *Ignavibacteria* (4.6%) quantity decreasing, *Actinobacteria* remaining the same fraction (16.7%) and small amounts of *Cyanobacteria* (4.6%) ZOTUs re-appearing. In the 30 cm deep layer, the composition becomes more diverse: *Proteobacteria* increase again (to 28.5%), similarly, with *Chloroflexi* (to 19.8%), *Firmicutes*, *Actinobacteria* and *Bacteroidetes* decrease (to 11.7%, 10.8% and 4.9%, respectively), *Cyanobacteria* remain (at 4.4%), and *Spirochaetes* (6.8%) and *Euryarchaeota* (5.9%) are observed.

AK mangroves phyla

At AK (Fig. 5c), the sediment surface layer is populated with *Proteobacteria* (40.6%), *Chloroflexi* (15.3%), *Bacteroidetes* (12.6%), *Euryarchaeota* (11.7%) and *Cyanobacteria* (5.2%). Deeper, at 5 cm, *Proteobacteria* remain as the dominant phylum (at 45.8%) while the *Chloroflexi* (7.9%) and *Euryarchaeota* (9.2%) ZOTUs percentage decreases, *Bacteroidetes* and *Cyanobacteria* increase slightly (14.9% and 10.8%, respectively) and a small amount of *Actinobacteria* (4.1%) is detected. At 11 cm depth, the portion of *Proteobacteria* falls

(to 26.2%), *Chloroflexi* increases (24.5%) and *Bacteroidetes* becomes less abundant. *Euryarchaeota* increases (to 17.0%) and *Spirochaetes* and *Plantomycetes* make up a small share (4.4% and 5.1%, respectively) of the ZOTUs at this depth. At the deepest 42 cm layer, *Proteobacteria* (26.7%), *Euryarchaeota* (21.0%), *Chloroflexi* (17.9%) and *Firmicutes* (13.0%) are the major phyla, while phyla at <4% abundance compose 21.3% of the ZOTUs.

KAAS salt pond genera

The major abundant genera in the coastal site sediments, which were greater than 4% of the total ZOTUs generated are shown in Fig. 6. At the genus level, the KAAS Salt Pond (Fig. 6a) surface layer at 0.3 cm is diverse, supporting chemoheterotrophs such as *Spirochaetes* (14.7%), sulfate-reducing bacteria from the genus *Desulfovibrio* (10.9%), the filamentous aerobic alphaproteobacterial genus *Alysiosphaera* (10.2%), the cyanobacterial genera *Coleofasciculus* (also known as *Microcoleus*; 10.1%) and *Lyngbya* (6.3%), the halophilic heterotrophic genus *Salisaeta* (4.8%) and the photosynthetic aerobic *Melittangium* (4.3%). At 4 cm depth in the core, the most populous genus is the chemotrophic halophile *Thermococcus*

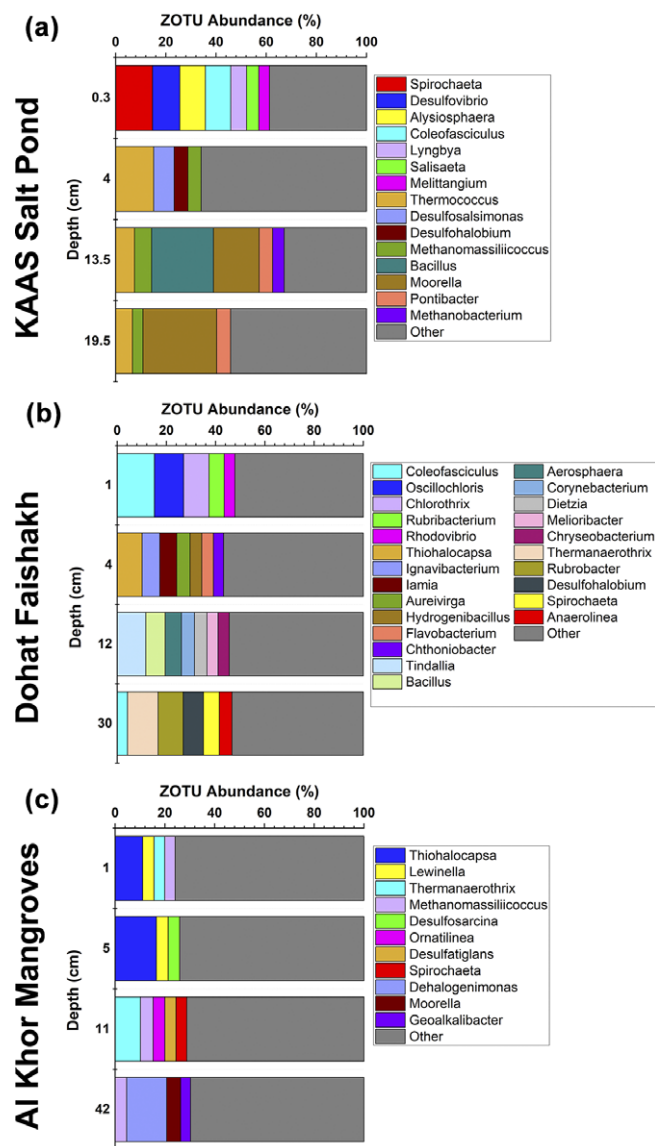


Figure 6. Genus-level taxonomic classification of ZOTU sequences: (a) KAAS Salt Pond site; (b) DF site; (c) AK site microbial genera. The 'Other' classification in grey represents the sum of ZOTUs with <4% abundance in the analysis.

(15.2%), followed by the sulfate-reducing bacterial genera *Desulfosalsimonas* (8.1%), *Desulfohalobium* (5.5%) and the methanogenic genus *Methanomassiliicoccus* (5.2%). At 13.5 cm depth, there appears an abundance of the facultative anaerobic fermenting genera *Bacillus* (24.6%) and *Moorella* (18.2%), a lower proportion of *Thermococcus* (7.5%), methanogenic archaeal genus *Methanomassiliicoccus* (6.9%), *Methanobacterium* (4.6%) and the strictly-aerobic genus *Pontibacter* (5.4%). At 19.5 cm in the sediment core, the ZOTUs are primarily dominated by *Moorella* (29.4%), with smaller fractions of *Thermococcus* (6.7%), *Pontibacter* (5.5%) and *Methanomassiliicoccus* (4.1%).

DF sabkha genera

In the DF site sediment (Fig. 6b), the abundant genera in the 1 cm deep layer were *Coleofasciculus* (15.1%), the photolithoautotrophic genus *Oscillochloris* (11.8%), the anoxygenic phototrophic *Chlorothrix* (10.3%), alkaliphilic *Rubribacterium* (6.2%) and the photoheterotrophic *Rhodovibrio* (4.4%). A 4 cm sediment depth sees

the appearance of diverse genera in the purple sulfur bacterium *Thiohalocapsa* (10.1%), the thermophilic anaerobe *Ignavibacterium* (7.2%), mesophilic *Iamia* (6.9%), the marine aerobic *Aureivirga* (5.4%), chemolithoautotrophic anaerobe *Hydrogenibacillus* (4.8%), aerobic genera of *Flavobacterium* (4.7%) and *Chthoniobacter* (4.1%). At 12 cm depth, the predominant genera consist of anaerobic alkaliphile *Tindallia* (11.6%), the diverse thermophilic genus *Bacillus* (7.9%), mesophilic *Aerosphaera* (6.6%), the halotolerant genus *Corynebacterium* (5.3%), aerobic alkaliphile *Dietzia* (5.0%), facultative anaerobe *Melioribacter* (4.6%) and chemoorganotrophic *Chryseobacterium* (4.5%). In the 30 cm deep layer, the abundant genus is the thermophilic anaerobe *Thermanaerotherix* (12.4%), followed by thermo- and radio-tolerant genus *Rubrobacter* (10.2%), the SRB genus *Desulfohalobium* (8.3%), anaerobic chemoheterotroph *Spirochaeta* (6.4%), strict anaerobic *Anaerolinea* (5.2%) and *Coleofasciculus* (4.1%).

AK mangroves genera

At the AK mangroves site (Fig. 6c), the sediment layer at 1 cm depth consists primarily of *Thiohalocapsa* (11.1%), with smaller fractions of the aerobic chemo-organotroph *Lewinella* (4.6%), *Thermanaerotherix* (4.3%) and *Methanomassiliicoccus* (4.2%). At 5 cm depth, the proportion of *Thiohalocapsa* increases slightly (16.5%), additionally containing *Lewinella* (4.8%) and the SRB genus *Desulfosarcina* (4.6%). At the 11 cm deep layer, *Thermanaerotherix* becomes the dominant genus (10.2%), along with *Methanomassiliicoccus* (5.1%), the anaerobic chemo-organotroph *Ornatilinea* (4.7%), SRB genus *Desulfatiglans* (4.5%) and *Spirochaeta* (4.4%). Near the bottom of the core at 42 cm depth, the organo-halophilic anaerobic *Dehalogenimonas* becomes the most abundant genus (16.0%), followed by the anaerobic fermenter *Moorella* (5.6%), *Methanomassiliicoccus* (4.6%) and the haloalkaliphilic *Geoalkalibacter* (4.0%).

Discussion

Geochemical conditions at the sediment–water interface promote blue carbon sequestration

The rapidly changing geochemical conditions throughout the sediment column surface influence carbon (C) sequestration by generating biogeochemical zones to efficiently sequester carbon. Zonation of marine coastal sediments generally follows a pattern: the oxic layer at the SWI and the sub-oxic zones immediately below, followed by a sulfidic (sulfate-reducing) zone, then, a methanogenic zone (LaRowe *et al.*, 2020). Our microsensor data supports and determines the occurrence of these zones in the Qatari coastal sedimentary environments.

The geomorphology and hydrology of each of the studied coastal environments and the immediate surface conditions can affect C sequestration capacity. The geomorphology of KAAS Salt Pond, an isolated alkaline saline water body, influences the movement of water and, potentially, the deposition of allochthonous carbon. KAAS Salt Pond, situated in the northwestern inner lagoon of KAAS, receives the least tidal influx from the entrance channel of the Arabian Gulf, yet has the highest water residence time (Rivers *et al.*, 2020). Conversely, the hydrology at the DF site indicated substantial tidal movement, which is a major driver of surficial allochthonous C deposition in coastal wetlands (Saintilan *et al.*, 2013; Van de Broek *et al.*, 2018). Similarly, AK mangrove sediment probably receives substantial tide-stream C inputs in addition to C sequestration in mangrove root growth and CO₂ capture (Alongi, 2014).

KAAS Salt Pond was overall less oxygenated at the SWI than the other sites and had on average the most negative redox potential of < -300 mV at 2 cm depth. The redox potential profile, as well as the appearance of the mat at the surface, closely resembles that of red microbial mats documented on the northern coast of KAAS, which were also alkaline and oxygen-undersaturated, with highly negative redox potential (DiLoreto *et al.*, 2019). High-temperature anoxic conditions protect surficial organic matter in coastal sediments from oxidative degradation and promote C sequestration (Trevathan-Tackett *et al.*, 2017). At the SWI, the peaking of sediment oxygen concentration can be attributed to oxygenic microbial respiration. The SWI at the DF site was the most oxygenated with the highest redox potential of the studied sites, increasing the oxidative degradation of OM. The AK mangroves were bioturbated by gastropods (Al-Khayat *et al.*, 2021), which may explain the considerable oxygen concentration at the SWI, even though no microbial mat was observed at this site. Oxic conditions were only present at the SWI, and anoxic, sulfidic conditions dominated the immediate subsurface sediment. Coastal mangrove sediments have among the highest rates of sulfate reduction and oxygen consumption of coastal ecosystems (Brodersen *et al.*, 2019), hence their massive potential for C mineralization.

Sub-surface sediment acidification, which we observed at all sites, is caused by organic matter mineralization through microorganisms. Anoxic conditions below the SWI promote microbial carbon mineralization via anaerobic microbial respiration of organic matter by sulfate reduction resulting in carbonate formation (Dupraz and Visscher, 2005; Vasconcelos *et al.*, 2014; Vasconcelos and Mckenzie, 1997a). The overall alkaline pH of the sediment is attributable to the high concentration of calcium and is supported by the sulfate reduction process, which uses up free H^+ to form H_2S and HCO_3^- . This process is a key factor in the creation of oversaturation conditions for the precipitation of calcium carbonate minerals, in addition to the EPS mineral-templating effect (Bontognali *et al.*, 2014; Braissant *et al.*, 2007). Maintenance of the sulfate-reduction rate is thus an important control on the dissolution and precipitation of carbonates in marine sediment (Zhang, 2020). The geochemical zones of the marine coastal sediments are therefore well-suited for carbon sequestration.

Comparison of sedimentary organic and inorganic carbon sequestration

KAAS salt pond

Each coastal site's sediment characteristics affect the route of organic and inorganic carbon sequestration. The KAAS Salt Pond site shares a similar depositional environment with other sites around KAAS (Rivers *et al.*, 2020). However, though studies of other KAAS sites report TOC around 2.0% at the SWI, the TOC% in the KAAS Salt Pond sediment (Fig. 4a) decreases below 0.5% at about 20 cm depth, while at a northeastern coastal site, it remains just above 1.0% until 35 cm depth (Al Disi *et al.*, 2023). Hydrodynamic transport of fine-grained sediment is known to have a positive correlation with sediment TOC in coastal flats (Zhao *et al.*, 2023). The effect of hydrodynamics is evident in KAAS: the sea's northeastern coast in the lagoon proximal to the entrance channel delta is rich in high-Mg calcite mud and hosts decimetre-thick organic-rich microbial mats at the SWI. Delta-distal supratidal regions of the inner lagoon have a predominantly siliciclastic composition with barely a centimetre thickness of surface microbial mat (Rivers *et al.*, 2020). Our PCA plot for KAAS Salt Pond (Figure S4A) visualizes a similar mechanism in that bulk density;

TOC, TIC, chlorophyll and phosphorus concentrations are governed solely by the depth and density of the sediment, and OM degradation does not strongly influence carbonate mineralization and carbon burial. In siliciclastic sedimentary environments, the diagenesis of opal-A to opal-CT uses up Mg^{2+} and inhibits dolomite formation, while transformation to quartz releases Mg^{2+} and promotes dolomitization (Baker and Kastner, 1981). In addition to bicarbonate anions provided by the sulfate reduction process, the above processes may explain the presence of dolomite at KAAS Salt Pond despite the low TOC content and OM degradation rates. The sum of C_{org} stock was the lowest at KAAS out of all sites. Sabkha sediments host low carbon stocks compared to the microbial mat and mangrove habitats in the same arid coastal region probably due to minimal hydrogeological and vegetative inputs (Carpenter *et al.*, 2023; Schile *et al.*, 2017). The rapid decline in TOC with depth at KAAS limits its availability as an energy source and has implications for microbial diversity. For example, the phylum *Firmicutes* commonly forms endospores to survive extreme, drought-like conditions, thus metagenomic approaches to understand their activities are recommended (Wunderlin *et al.*, 2014). Aeolian deposition of clay is commonplace in KAAS (Rivers *et al.*, 2020) and Mg-carbonates have been shown to form in close association with clay minerals such as montmorillonite and palygorskite in the sediment matrix (Liu *et al.*, 2019; Perri *et al.*, 2018). Though our XRD analysis did not identify abundant clay minerals in the sediment, high Mg/Ca ratios of the porewater observed at KAAS (Figure S2A) and the interaction with buried clays are probably triggers for the formation of dolomite, among other biogeochemical factors. A study of the alkaline Daihai Lake in China found that groundwater Ca^{2+} concentration and permeability of the SWI were the major factors slowing the recharge rate of groundwater-dissolved inorganic carbon to lake water (Dong *et al.*, 2023). Our PCA showed the same mechanism, in that C sequestration was dictated primarily by the sediment depth and density. The efflux of carbon at KAAS Salt Pond would probably be extremely slow due to the consolidated silty surface layers, the dense microbial mat at the SWI and the high porewater Ca^{2+} , ensuring saturation of the carbonate minerals. Similarly, in shallow alkaline salt lakes the main factor affecting carbonate formation is the binding capacity of cyanobacterial EPS, with the phototrophic CO_2 fixation rate a secondary consideration (Arp *et al.*, 1999). So, because KAAS Salt Pond is isolated from geophysical or anthropogenic perturbations, slow carbon loss is probably balanced by slow carbonate mineralization.

DF sabkha

Conversely, the DF supratidal zone is composed of mostly carbonate-rich sediment. The DF TOC profile is similar to that reported in previous studies (Al Disi *et al.*, 2023; Brauchli *et al.*, 2016): the TOC% sharply increases at about 13 cm depth and, again, at 35 cm depth. The C_{org} stock at DF is nearly double that of the KAAS site for the top 35 cm of sediment; direct hydrogeological input of OM to DF sediments from tidal groundwater is probably a major influencing factor. The localization of organic carbon at greater sediment depths in coastal environments has been suggested to be due to OM–mineral interactions with dolomite and the preservation of microbial mats. Interactions with buried microbial mats, living or dead, facilitate the mineralization of dolomite through templating on carboxyl functional groups (Brauchli *et al.*, 2016; Fan *et al.*, 2023). The intensity of dolomite characteristic peaks in the XRD spectrum of DF sediment increases with increasing depth, while the peaks of gypsum become diminished with

depth (Fig. 4b). In a carbonate-saturated fluid, gypsum can rapidly dissolve and re-mineralize to calcite, vaterite and aragonite (Azdarpour *et al.*, 2018; Yu *et al.*, 2019), providing another route for the nucleation and maturation of carbonates and liberating sulfate for use in reduction processes, which in turn promotes carbonate mineralization. It was also shown that gypsum crystals found at DF can host encapsulated organic matter (DiLoreto *et al.*, 2023). In addition to presenting a stable form of OM sequestration which could explain the high TOC% at depths with abundant gypsum, such an interaction can further catalyze dolomite nucleation upon OM release after gypsum dissolution. Though buried cyanobacterial mats are probably a major contributor to the OM at greater sediment depth, future studies measuring $\delta^{13}\text{C}$ isotopes of the sediment would shed more light on the sources of organic carbon and their contribution to the blue carbon sequestered at DF. C_{org} stock values reported for sabkhas along Saudi Arabia's east coast of the Persian Gulf were roughly 1.5x the C_{org} stock observed in young mangroves along the same coastline (Cusack *et al.*, 2018), similar to the results observed here (extrapolated to the same depth).

It has been suggested that OM degradation is one of the driving forces behind dolomite nucleation (Sanz-Montero *et al.*, 2019; Vasconcelos and Mckenzie, 1997b) and that OM degradation is elevated at the buried microbial mat depths at DF (Brauchli *et al.*, 2016). The high C:N (>70) at 10–20 cm sediment depth (Fig. 4b) suggests that it is indeed a highly degradative environment favourable for dolomite mineral formation, which is also observed at these depths. Our PCA results support the role of OM degradation in dolomitization. At the DF site, the TOC, TIC and C:N eigenvectors are aligned to one PC (Figure S4B), suggesting a strong correlation between C:N and TIC/TOC content, unlike the KAAS Salt Pond. Dolomite has been observed mineralizing in buried and surficial microbial mats in a sabkha near Abu Dhabi (UAE) (Bontognali *et al.*, 2010), having similar O_2 and H_2S microsensors depth profiles as those reported for DF sabkha in the present study (Fig. 3b), though DF is roughly twice as oxygenated at the SWI. Though the presence of H_2S within the Abu Dhabi mat indicates localized sulfate depletion, which should remove dolomite precipitation inhibition, the study researchers affirm that modern dolomite mineralization to the observed extent is unrealistic as sulfate depletion cannot be reliably maintained. Rather, they claim that dolomite probably precipitates through the EPS-templating mechanism, as dolomite is also present in supratidal buried mats which do not show any current significant microbial activity. Similarly, in the present study, at DF there is a buried laminated microbial mat component about 15 cm below the SWI where dolomite is readily precipitating, as seen by its presence in the XRD spectra of the surface, 11 cm and 34 cm layer from DF (Fig. 4b). An “organogenic” model is thus very likely to be the mechanism by which dolomite precipitates in these settings, with influence from sulfate-reduction processes and also microbial carbon cycling, as discussed in the section below on the Role of microorganisms in blue carbon cycling and sequestration.

AK mangroves

Mangrove sediments are effective coastal carbon preservation environments as they uptake carbon from a variety of auto- and allochthonous sources. In young, low-elevation intertidal mangroves, the main C input to the sediment is of allochthonous origin due to greater tidal influx and thus greater suspended sediment transport and deposition (Suello *et al.*, 2022). In addition to mangrove plant sources of TOC in intertidal mangrove sediments, there

are large TOC inputs from marine algal sources, which have a distinct $\delta^{13}\text{C}$ signature and lower TOC:TN in the surface sediments (Tang *et al.*, 2023). The observed C:N ratio of the AK surface sediment layers is considerably lower than downcore C:N (Fig. 4c). Thus, it is likely that allochthonous microbial biomass is a major source of organic carbon at the AK sediment surface while, at deeper layers, the mangrove plant matter makes a greater contribution to TOC. On the other hand, the roots of the mangroves may provide tunnels for oxygen diffusion and lead to the degradation of organic matter. Such a mechanism of blue carbon burial at AK is supported by our PCA (Figure S4C) in that the TOC, TP and chlorophyll concentration eigenvectors are aligned in the opposite direction as C:N, sediment depth and TIC eigenvectors on PC1, while TOC is aligned with C:N and sediment depth on PC2 suggesting that burial and degradation of surficial organic material at increasing depths is correlated with inorganic carbon sequestration.

Unlike the DF site, where TOC, C:N and dolomite XRD peak intensity all increase as depth increases (Fig. 4b), at AK the TOC decreases to a minimum while C:N increases at 20 cm depth, while also increasing in dolomite XRD peak intensity (Fig. 4c), suggesting that dolomite mineralization is linked to sedimentary OM degradation in coastal environments, not just the presence of organic matter (Brauchli *et al.*, 2016). Additionally, the increase in the downcore C:N ratio is probably a result of SRB and fermenter microbial metabolism degrading the sinking surficial OM, with both processes together contributing to the re-mineralization of carbonates (Dupraz and Visscher 2005). Dolomite can thus be considered an effective inorganic C sequestration end-product in coastal sediments where OM degradation allows it to nucleate. Observation of stoichiometric dolomite rhombs in SEM-EDXS (Figure S3) and the depletion of Mg relative to Ca in the porewater throughout the AK core (Figure S2C) suggests the *de novo* formation of proto-dolomite in the mangrove environment rather than by gradual remineralization of aragonite.

TP and chlorophyll at all coastal sites

To date, mineralogical studies of KAAS, DF and AK sediment have reported no evidence of phosphate minerals (Al Disi *et al.*, 2023; Brauchli *et al.*, 2016). Our XRD data showed that no major peaks corresponding to phosphate minerals were detected in XRD at any site, thus the major forms of P in the sediment are assumed to be organic and polymeric phases such as polyP, which has been documented previously at KAAS (DiLoreto *et al.*, 2019). It is possible that phosphate mineral peak signatures are masked by more abundant carbonate and silicate mineral peaks, thus, for future studies, a sequential extraction (SEDEX) (Ruttenberg, 1992) and measurement of P phases is recommended, which would additionally clarify P fraction contents. Our TP profile at all the studied sites supports the prevalence of P as organic matter, as it rises and falls in relation to the TOC at each site (Fig. 4, Table S1). Total chlorophyll concentration was highest at the layers nearest to the SWI at all sites (Fig. 4), with the highest surface chlorophyll concentration (100.3 ng chlorophyll/g sediment) observed at 0.5 cm depth at KAAS Salt Pond (Fig. 4a), followed by 1 cm depth at DF (18.3 ng/g) (Fig. 4b) and 1 cm depth at AK (1.6 ng/g) (Fig. 4c). Heightened coastal sediment chlorophyll concentration is commonly a response to ocean acidification and increased $p\text{CO}_2$, which shifts the microbial community composition toward anoxygenic phototrophy (Mandal *et al.*, 2021; Mazière *et al.*, 2022). An exception exists in high-competition ecosystems, despite alkaline conditions such as the KAAS surface microbial mats where microbial community cooperation by heterotrophic microbes can support

phototrophy (Dupraz and Visscher, 2005; Mandal *et al.*, 2021). Notably, the relative concentration of chlorophyll types at the SWI differed between sites; the KAAS surface layer contained 86.0% chlorophyll-*a*, 1.7% chlorophyll-*b* and 12.3% chlorophyll-*c*, while the DF surface was composed of 63.8%, 11.5% and 24.7% and AK surface composed of 73.8%, 13.4% and 12.8% of chlorophyll-*a*, -*b* and -*c*, respectively. Chlorophyll-*c* is abundantly present in marine photosynthetic organisms, so it is fitting that the DF site has the highest proportion of chlorophyll-*c*, being located directly in the coastal intertidal zone. Increased chlorophyll-*a* relative to chlorophyll-*b* at KAAS suggests an adaptation to intense light irradiation as chlorophyll-*b* is primarily synthesized in low-light conditions to absorb more blue light (Dale and Causton, 1992). Chlorophyll has been found to be preserved inside evaporitic gypsum minerals in the DF subsurface sediment (DiLoreto *et al.*, 2023). The greater overall abundance of all chlorophylls at KAAS is supported by the abundance of oxygenic and anoxygenic phototrophic bacteria found at nearby sites in the sabkha (DiLoreto *et al.*, 2019, 2021). Oxygenic and anoxygenic phototrophic activity at the SWI fixes atmospheric CO₂ and produces EPS, increasing SOC and promoting other microbial community functions, as described in the following section.

Role of microorganisms in blue carbon cycling and sequestration

The microorganisms in the coastal sediment contribute to carbon cycling and sequestration by driving the degradation of organic carbon. Species of anoxygenic phototrophs such as *Proteobacteria* and *Chloroflexi* have been found to promote carbon dioxide fixation in hypersaline coastal sediments (Klatt *et al.*, 2013; Lenk *et al.*, 2011). Members of these phyla have been documented as major inhabitants of mangrove sediments (Hu *et al.*, 2022). Similarly, in our study, these two phyla were found throughout the sediment cores at all sites, primarily in the surface layers along with *Cyanobacteria*, suggesting the use of the Calvin-Benson (CB) cycle for photoautotrophic carbon fixation from CO₂. This process is probably important at the DF site where *Cyanobacteria* and *Chloroflexi* make up more than half of all observed phyla in the surface layer (Fig. 5b). A higher overall proportion of *Firmicutes* in the sediment core layers was found at the two sites with surface microbial mats, KAAS Salt Pond and DF, supporting the idea that *Firmicutes* have a crucial role in deep sediment microbial biomass carbon cycling in coastal environments (Fernandez *et al.*, 2016). Members of phylum *Firmicutes* have been shown to use the CB cycle and the reductive acetyl-CoA pathway for CO₂ fixation (Frolov *et al.*, 2019). The phylum *Firmicutes* has been attributed to inducing precipitation of Mg-rich carbonate minerals in decaying microbial mats from alkaline lakes using EPS as a mineralization surface (Sanz-Montero *et al.*, 2019). At all our studied sites, *Firmicutes* were found in the deeper sediment core layers (Fig. 5), and the same sediment depths were also rich in dolomite (Fig. 4). Given that *Firmicutes* also participate in dissimilatory sulfate reduction (Song *et al.*, 2021; Wasmund *et al.*, 2017), oxidizing organic carbon and producing CO₂, they are probably key facilitators in the cycling, sequestration and re-mineralization of carbon in coastal sediment. Throughout the AK site layers, the sequenced genera of less than 4% abundance are consistently between 70–75% of total sequences, while at DF and KAAS Salt Pond, the less abundant sequences consist between 30–60% of total ZOTUs. This may reflect the established microbial mat communities present at DF and KAAS compared to AK.

Specific microbial genera are known to contribute to sediment carbon sequestration and cycling. Members of the cyanobacterial genus *Coleofasciculus* (formerly *Microcoleus*), which we found abundantly at the KAAS and DF surface microbial mat layers (Fig. 6a–b), use carbonic anhydrase enzymes to quickly catalyze CO₂ hydration to carbonic acid (HCO₃⁻) (Heuer *et al.*, 2021). Under alkaline conditions, such as those observed at the SWI of KAAS and DF sites (Fig. 3a–b), HCO₃⁻ can dissociate to CO₃²⁻ and H⁺ and combine with Ca²⁺ to precipitate CaCO₃. At night, in hypersaline microbial mats, *Coleofasciculus* also ferments photosynthates to organic acids under anoxic, dark conditions – which are taken up by *Chloroflexi* and stored intracellularly as polyhydroxyalkanoate (PHA) (Burow *et al.*, 2013). Members of the genus *Rubrobacter*, a thermophile residing at 30 cm depth in DF, are also known to store PHA to tolerate extreme conditions (Kourilová *et al.*, 2021). Accumulation of PHA as a form of carbon capture is heavily favoured in lower pH, vegetated conditions where microbial diversity is low (Grey *et al.*, 2023), therefore intracellular PHA storage is probably a major contributor to microbial carbon sequestration at AK and DF but not KAAS, which hosts markedly less *Chloroflexi* (Fig. 5a). *Cyanobacteria* and *Chloroflexi* phyla combined make up roughly half of the observed ZOTUs at the DF surface, a third at KAAS and a quarter of the total at AK (Fig. 5a–c) – thus a similar mechanism of organic carbon cycling and sequestration is possible. The cyanobacterial genus *Lyngbya* is found to prefer long-term carbon storage by utilizing sequestered CO₂ and HCO₃⁻ for carbohydrate and lipid molecule synthesis (Murdock, 2016). The photolithoautotrophic purple sulfur bacterial genus, *Thiohalocapsa*, was abundant at the surface of the AK site. *Thiohalocapsa* has been shown to uptake acetate – a product of OM degradation – for growth, performs CO₂ fixation and is essential to the function of the coastal sediment microbial community (Hubas *et al.*, 2017). Proximity to residential areas and industrial development may be an additional cause for the relatively ‘young’ microbiome at AK. The genus *Lewinella* is common to mangrove sediments that undergo vegetative dieback, performing key degradation functions for the mangrove rhizobiome (Wainwright *et al.*, 2023), using products of cellulose hydrolysis as carbon and energy sources. However, *Lewinella* does not use other substrates such as citrate, acetate, formate and pyruvate (Song *et al.*, 2021), leaving them available for carbon fixation processes by other microbes. Overall, the abundance of sulfate-reducing bacteria (*e.g.*, *Desulfosarcina*, *Desulfohalobium*, *Desulfatiglans*, *Desulfosalsimonas*, *Geoalkalibacter*) and fermenters (*e.g.*, *Moorella Bacillus*) in the deeper sediment across the studied sites ensures the degradation of SOM to labile low-molecular weight carbon sources and carbonate mineral precursors, favouring the nucleation of disordered dolomite phases (Dunham *et al.*, 2020; Dupraz and Visscher, 2005).

The increase in the proportion of archaea with sediment depth could potentially have an impact on sediment carbon biogeochemistry in the coastal areas surrounding Qatar. Archaea are known to inhabit extreme, hypersaline and especially vegetated wetland environments. Archaea are more populous and better suited to inhabit anoxic, subsurface sediment depths than bacteria and thus usually increase in proportion with increasing depth (Zhang *et al.*, 2023). Archaeal metabolisms are very diverse, which allows them to participate in many aspects of blue carbon cycling. For example, the predominant fraction of carbon-associated functional genes in China’s coastal wetland sediments is sourced from archaea (Yang *et al.*, 2022), with the genes encoding enzymes involved in sediment carbon cycling processes with high functional redundancy and diversity. Archaea also take part in denitrification, methanogenesis

and methane oxidation. Members of the phylum *Euryarchaeota* were able to degrade a variety of anthropogenic-pollutant hydrocarbons found in Sundarban (India) mangrove sediments due to their metabolic versatility (Mukherji *et al.*, 2020). Archaeal hydrocarbon capture and degradation is thus a promising C bioremediation application. In alkaline cyanobacterial mats, extreme halophilic archaea utilize acid metabolites of *Coleofasciculus chthonoplastes* respiration as a C energy source (Andrei *et al.*, 2012). Bacterial–archaeal interactions in hypersaline sediments are so common that shared nutrient availability indicators (such as TP and organic C/N) are better predictors of co-occurrence than other individual geochemical influencing factors such as salinity (Wang *et al.*, 2021). The documented extremophilic, opportunistic and versatile nature of *Euryarchaeota* explains their presence in the Qatari coastal sediment and co-existence among bacteria with similar or compatible metabolisms. High spatial resolution metagenomic analyses of the sediment column at the coastal sites will be able to clarify the bacterial and archaeal metabolic activities and pathways pertaining to blue carbon sequestration.

Organic matter–mineral interactions in blue carbon sequestration

Organic matter–mineral interactions have been suggested as one of the central influences in the diagenesis of sedimentary carbonate minerals. Dolomite has sparked particular interest due to its abundant occurrence in the geological record, but limited modern formation in evaporitic environments such as sabkhas. Recently, dolomite formation stabilized by OM concentrated by coastal microbial communities has been observed as a type of microbially-influenced “organomineralization”, which significantly decreases dolomite mineralization time by the order of several million years (by authigenic precipitation from saturated seawater) to only a few years. Studies of hypersaline sediments have concluded that Ca^{2+} and Mg^{2+} ions have high binding affinity to microbial EPS due to their surface interaction with negatively charged functional groups such as carboxylic acids (Braissant *et al.*, 2007; Krause *et al.*, 2012; Petrash *et al.*, 2017). Laboratory experiments have shown that by removing the Mg^{2+} ion’s hydration shell, Mg^{2+} incorporation into calcite and precipitation of disordered dolomite is induced (Fang *et al.*, 2022). Thus, similar to how blue carbon is captured from the atmosphere or tidal influx and cycled through the sediment microbial community, blue carbon can be incorporated and sequestered into a stable inorganic carbonate phase through organomineralization. Furthermore, EPS can be considered a template or catalyst to direct and overcome kinetic barriers to dolomite mineralization. Our STXM findings (Figure S5) of dolomite and EPS-carboxylate co-localization strongly suggest that such a calcite transformation or dolomite maturation mechanism by interaction with EPS is occurring presently in the DF sediment. Similarly, negatively charged surfaces of clay minerals such as montmorillonite can also open the Ca^{2+} and Mg^{2+} hydration shell by binding them electrostatically and inducing proto-dolomite precipitation (Liu *et al.*, 2019). Our TEM-EDXS map shows a disordered dolomite mineral particle crystallizing from the surface of a Mg- and Si-rich sediment matrix (Figure S6), though the identity of the matrix was not confirmed. Although inorganic carbon precipitated as dolomite, aragonite or calcite is relatively stable, any massive physical change sustained to the SWI of coastal sediments can cause profound changes to the sediment composition and microbial community, impacting the capture and cycling of blue carbon.

Coastal blue carbon stores are threatened by rapid climate change and land-use changes. Increases in industrial greenhouse gas emissions will put pressure on each of the unique ecosystems studied here to sequester more carbon. At the same time, ecosystem destruction through land development will hinder blue carbon sequestration and release stored blue carbon into the atmosphere and marine ecosystems. KAAS and DF sites are recognized national conservation areas but are commonly used for motorized recreation by Qatari residents. The AK mangroves site is proximal to the town of Al Khor, which is presently undergoing residential and commercial land development. Care must be taken to avoid impacting the natural blue carbon sequestration abilities of these coastal regions.

Conclusion

Our biogeochemical observations indicate that carbon cycling and sequestration in three unique coastal environments in Qatar are governed to differing degrees by hydrodynamic deposition, oxic/anoxic and sulfidic conditions, OM degradation and inorganic carbon phases and the microbial community composition. Correlations were revealed linking TOC and TIC to the OM degradation rate at Dohat Faishakh sabkha, where disordered dolomite phases were found nucleating in close proximity to buried microbial mat OM by STXM and TEM. At an isolated salt lake at Khor Al Adaid sabkha, the TOC, TIC and TP are only linked with sediment depth, and carbon is probably kept sequestered beneath a highly alkaline protective sediment–water interface where oxygenic and anoxygenic phototrophy fixes carbon dioxide as organic carbon in a dense surficial microbial mat. At the Al Khor mangroves, TIC is correlated to the burial of mangrove-derived degraded OM, and XRD reveals dolomite mineral abundant in the surface sediments. A complex microbial community ranging from anoxygenic phototrophs and SOB near the SWI and SRB, fermenting bacteria down-core capturing auto- and allochthonous carbon, degrading, cycling and sequestering it through complementary action, probably provide the necessary conditions for the organomineralization of dolomite in the Qatari coastal sediments.

Supplementary material. To view supplementary material for this article, please visit <http://doi.org/10.1180/gbi.2024.8>.

Acknowledgements. Jassim Abdulla A Al-Khayat (University of Qatar, Doha) and Maria Dittrich (University of Toronto) would like to acknowledge the Qatar National Research Fund (a member of Qatar Foundation) for the Grant NPRP12S-0313-190349. Maria Dittrich was also supported by the National Sciences and Engineering Research Council of Canada (NSERC Discovery Grant, RGPIN-06184) and the Canada Foundation for Innovation and Ontario Research Fund (Leaders Opportunity Fund, Grant Number 22404) for supervision of the graduate thesis by Ivan Strakhov. We would like to thank Dr Kim Tait and Veronica Di Cecco at the Royal Ontario Museum Centre for Applied Planetary Mineralogy for the Bruker D8 Advance training.

References

- Al-Khayat, J.A., Vethamony, P. and Nanajkar, M. (2021) Molluscan diversity influenced by mangrove habitat in the Khors of Qatar. *Wetlands*, **41**(4), 1–19. <https://doi.org/10.1007/s13157-021-01441-6>
- Al Disi, Z.A., Naja, K., Rajendran, S., Elsayed, H., Strakhov, I., Al-Kuwari, H. A. S., Sadooni, F., Dittrich, M. and Al-Khayat, J.A. A. (2023) Variability of blue carbon storage in arid evaporitic environment of two coastal Sabkhas or mudflats. *Scientific Reports*, **13**(12723), 1–12. <https://doi.org/10.1038/s41598-023-39762-7>

- Alongi, D.M. (2014) Carbon cycling and storage in mangrove forests. *Annual Review of Marine Science*, **6**, 195–219. <https://doi.org/10.1146/annurev-marine-010213-135020>
- Andrei, A. Ş., Banciu, H.L. and Oren, A. (2012) Living with salt: Metabolic and phylogenetic diversity of archaea inhabiting saline ecosystems. *FEMS Microbiology Letters*, **330**(1), 1–9. <https://doi.org/10.1111/j.1574-6968.2012.02526.x>
- Areias, C., Barbosa, C.F., Cruz, A.P. S., McKenzie, J.A., Ariztegui, D., Eglinton, T., Haghipour, N., Vasconcelos, C. and Sánchez-Román, M. (2022) Organic matter diagenesis and precipitation of Mg-rich carbonate and dolomite in modern hypersaline lagoons linked to climate changes. *Geochimica et Cosmochimica Acta*, **337**, 14–32. <https://doi.org/10.1016/j.gca.2022.09.030>
- Arp, G., Reimer, A. and Reitner, J. (1999) Calcification in cyanobacterial biofilms of alkaline salt lakes. *European Journal of Phycology*, **34**(4), 393–403. <https://doi.org/10.1017/S0967026299002292>
- Avnimelech, Y., Ritvo, G., Meijer, L.E. and Kochba, M. (2001) Water content, organic carbon and dry bulk density in flooded sediments. *Aquacultural Engineering*, **25**, 25–33.
- Azdarpor, A., Afkhami Karaei, M., Hamidi, H., Mohammadian, E. and Honarvar, B. (2018) CO₂ sequestration through direct aqueous mineral carbonation of red gypsum. *Petroleum*, **4**(4), 398–407. <https://doi.org/10.1016/j.petlm.2017.10.002>
- Baker, P.A. and Kastner, M. (1981) Constraints on the formation of sedimentary dolomite. *Science*, **213**(4504), 214–216.
- Bauer, J.E., Cai, W.J., Raymond, P.A., Bianchi, T.S., Hopkinson, C.S. and Regnier, P.A. G. (2013) The changing carbon cycle of the coastal ocean. *Nature*, **504**(7478), 61–70. <https://doi.org/10.1038/nature12857>
- Bontognali, T.R.R., Vasconcelos, C., Warthmann, R.J., Bernasconi, S.M., Dupraz, C., Strohmenger, C.J. and McKenzie, J.A. (2010) Dolomite formation within microbial mats in the coastal sabkha of Abu Dhabi (United Arab Emirates). *Sedimentology*, **57**(3), 824–844. <https://doi.org/10.1111/j.1365-3091.2009.01121.x>
- Bontognali, T.R.R., McKenzie, J.A., Warthmann, R.J. and Vasconcelos, C. (2014) Microbially influenced formation of Mg-calcite and Ca-dolomite in the presence of exopolymeric substances produced by sulphate-reducing bacteria. *Terra Nova*, **26**(1), 72–77. <https://doi.org/10.1111/ter.12072>
- Braissant, O., Decho, A.W., Dupraz, C., Glunk, C., Przekop, K.M. and Visscher, P.T. (2007) Exopolymeric substances of sulfate-reducing bacteria: Interactions with calcium at alkaline pH and implication for formation of carbonate minerals. *Geobiology*, **5**(4), 401–411. <https://doi.org/10.1111/j.1472-4669.2007.00117.x>
- Brauchli, M., McKenzie, J.A., Strohmenger, C.J., Sadooni, F., Vasconcelos, C. and Bontognali, T.R. R. (2016) The importance of microbial mats for dolomite formation in the Dohat Faishakh sabkha, Qatar. *Carbonates and Evaporites*, **31**(3), 339–345. <https://doi.org/10.1007/s13146-015-0275-0>
- Brodersen, K.E., Trevathan-Tackett, S.M., Nielsen, D.A., Connolly, R.M., Lovelock, C.E., Atwood, T.B. and Macreadie, P.I. (2019) Oxygen consumption and sulfate reduction in vegetated coastal habitats: Effects of physical disturbance. *Frontiers in Marine Science*, **6**, 1–13. <https://doi.org/10.3389/fmars.2019.00014>
- Burchette, T.P. (2012) Carbonate rocks and petroleum reservoirs: A geological perspective from the industry. *Geological Society Special Publication*, **370**(1), 17–37. <https://doi.org/10.1144/SP370.14>
- Burns, S.J., McKenzie, J.A. and Vasconcelos, C. (2000) Dolomite formation and biogeochemical cycles in the Phanerozoic. *Sedimentology*, **47** (SUPPL. 1), 49–61. <https://doi.org/10.1046/j.1365-3091.2000.00004.x>
- Burow, L.C., Woeikens, D., Marshall, I.P. G., Lindquist, E.A., Bebout, B.M., Prufert-Bebout, B.M., Hoehler, T.M., Tringe, S.G., Pett-Ridge, J., Weber, P.K., Spormann, A.M. and Singer, S.W. (2013) Anoxic carbon flux in photosynthetic microbial mats as revealed by metatranscriptomics. *The ISME Journal*, **7**(4), 817–829. <https://doi.org/10.1038/ismej.2012.150>
- Carpenter, S., Evans, C., Pittman, S.J., Antonopoulou, M., Bejarano, I., Das, H.S., Möller, M., Peel, K., Samara, F., Stamoulis, K.A. and Mateos-Molina, D. (2023) Multi-habitat carbon stock assessments to inform nature-based solutions for coastal seascapes in arid regions. *Frontiers in Marine Science*, **10**, 1–17. <https://doi.org/10.3389/fmars.2023.1239904>
- Cusack, M., Saderna, V., Arias-Ortiz, A., Masqué, P., Krishnakumar, P.K., Rabaoui, L., Qurban, M.A., Qasem, A.M., Prihartato, P., Loughland, R.A., Elyas, A.A. and Duarte, C.M. (2018) Organic carbon sequestration and storage in vegetated coastal habitats along the western coast of the Arabian Gulf. *Environmental Research Letters*, **13**(7). <https://doi.org/10.1088/1748-9326/aac899>
- d'Abzac, P., Bordas, F., Joussein, E., van Hullebusch, E.D., Lens, P.N. L. and Guibaud, G. (2013) Metal binding properties of extracellular polymeric substances extracted from anaerobic granular sludges. *Environmental Science and Pollution Research*, **20**(7), 4509–4519. <https://doi.org/10.1007/s11356-012-1401-3>
- Dale, M.P. and Causton, D.R. (1992) Use of the chlorophyll a/b ratio as a bioassay for the light environment of a plant. *Functional Ecology*, **6**(2), 190. <https://doi.org/10.2307/2389754>
- DiLoreto, Z.A., Bontognali, T.R. R., Al Disi, Z.A., Al-Kuwari, H.A. S., Williford, K.H., Strohmenger, C.J., Sadooni, F., Palermo, C., Rivers, J.M., McKenzie, J. A., Tuite, M. and Dittrich, M. (2019) Microbial community composition and dolomite formation in the hypersaline microbial mats of the Khor Al-Adaid sabkhas, Qatar. *Extremophiles*, **23**(2), 201–218. <https://doi.org/10.1007/s00792-018-01074-4>
- DiLoreto, Z.A., Garg, S., Bontognali, T.R. R. and Dittrich, M. (2021) Modern dolomite formation caused by seasonal cycling of oxygenic phototrophs and anoxygenic phototrophs in a hypersaline sabkha. *Scientific Reports*, **11**(1), 1–13. <https://doi.org/10.1038/s41598-021-83676-1>
- DiLoreto, Z.A., Ahmad, M.S., Al Saad Al-Kuwari, H., Sadooni, F., Bontognali, T. R. R. and Dittrich, M. (2023) Raman spectroscopic and microbial study of biofilms hosted gypsum deposits in the hypersaline wetlands: Astrobiological perspective. *Astrobiology*, **23**(9), 991–1005. <https://doi.org/10.1089/ast.2023.0003>
- Dong, S., Liu, B., Ma, M., Lei, J., Zhang, M. and Feng, Y. (2023) Influence mechanism of groundwater on the carbon cycle in alkaline lakes. *Journal of Hydrology*, **617** (PC), 129104. <https://doi.org/10.1016/j.jhydrol.2023.129104>
- Dunham, E.C., Fones, E.M., Fang, Y., Lindsay, M.R., Steuer, C., Fox, N., Willis, M., Walsh, A., Colman, D.R., Baxter, B.K., Lageson, D., Mogk, D., Rupke, A., Xu, H. and Boyd, E.S. (2020) An Ecological Perspective on Dolomite Formation in Great Salt Lake, Utah. *Frontiers in Earth Science*, **8**(24), 1–18. <https://doi.org/10.3389/feart.2020.00024>
- Dupraz, C. and Visscher, P.T. (2005) Microbial lithification in marine stromatolites and hypersaline mats. *TRENDS in Microbiology*, **13**(9), 429–438. <https://doi.org/10.1016/j.tim.2005.07.008>
- Eid, E.M., Arshad, M., Alrumman, S.A., Al-Bakre, D.A., Ahmed, M.T., Almahsheer, H. and Keshta, A.E. (2022) Evaluation of soil organic carbon stock in coastal sabkhas under different vegetation covers. *Journal of Marine Science and Engineering*, **10**(9). <https://doi.org/10.3390/jmse10091234>
- EMSL (1993) *Method 365.1, Revision 2.0: Determination of Phosphorus by Semi-Automated Colorimetry* (Issue August). https://www.epa.gov/sites/production/files/2015-08/documents/method_365-1_1993.pdf
- Fan, Q., Liu, D., Papineau, D., Qiu, X., Wang, H., She, Z. and Zhao, L. (2023) Precipitation of high Mg-calcite and protodolomite using dead biomass of aerobic halophilic bacteria. *Journal of Earth Science*, **34**(2), 456–466.
- Fang, Y., Zhang, F., Farfan, G.A. and Xu, H. (2022) Low-temperature synthesis of disordered dolomite and high-magnesium calcite in ethanol – water solutions: The solvation effect and implications. *ACS Omega*, **7**, 281–292. <https://doi.org/10.1021/acsomega.1c04624>
- Fernandez, A.B., Rasuk, M.C., Visscher, P.T., Contreras, M., Novoa, F., Poire, D. G., Patterson, M.M., Ventosa, A. and Farias, M.E. (2016) Microbial diversity in sediment ecosystems (evaporite domes, microbial mats, and crusts) of Hypersaline Laguna Tebenquiche, Salar de Atacama, Chile. *Frontiers in Microbiology*, **7** (AUG), 1–18. <https://doi.org/10.3389/fmicb.2016.01284>
- Frolov, E.N., Kublanov, I.V., Toshchakov, S.V., Lunev, E.A., Pimenov, N.V., Bonch-Osmolovskaya, E.A., Lebedinsky, A.V. and Chernyh, N.A. (2019) Form III RubisCO-mediated transaldolase variant of the Calvin cycle in a chemolithoautotrophic bacterium. *Proceedings of the National Academy of Sciences of the United States of America*, **116**(37), 18638–18646. <https://doi.org/10.1073/pnas.1904225116>
- Grey, A., Costeira, R., Lorenzo, E., O'Kane, S., McCaul, M.V., McCarthy, T., Jordan, S.F., Allen, C.C. R. and Kelleher, B.P. (2023) Biogeochemical properties of blue carbon sediments influence the distribution and monomer composition of bacterial polyhydroxyalkanoates (PHA). *Biogeochemistry*, **162**(3), 359–380. <https://doi.org/10.1007/s10533-022-01008-5>
- Heuer, J., Kraus, Y., Vučak, M. and Zeng, A.P. (2021) Enhanced sequestration of carbon dioxide into calcium carbonate using pressure and a carbonic

- anhydrase from alkaliphilic Coleofasciculus chthonoplastes. *Engineering in Life Sciences*, **22**(3–4), 178–191. <https://doi.org/10.1002/elsc.202100033>
- Howard, J., Hoyt, S., Isensee, K., Telszewski, M. and Pidgeon, E. (eds.) (2014) *Coastal Blue Carbon: Methods for assessing carbon stocks and emissions factors in mangroves, tidal salt marshes, and seagrasses*. Conservation International, Intergovernmental Oceanographic Commission of UNESCO, International Union for Conservation of Nature. Arlington, Virginia, USA.
- Hu, B., Liao, J., Zhang, Q., Ding, S., He, M., Qiao, Y., Zhang, Z., Shang, C. and Chen, S. (2022) Diversity and vertical distribution of sedimentary bacterial communities and its association with metal bioavailability in three distinct mangrove reserves of South China. *Water*, **14**(971), 1–27. <https://doi.org/10.3390/w14060971>
- Hubas, C., Boeuf, D., Jesus, B., Thiney, N., Bozec, Y. and Jeanthon, C. (2017) A nanoscale study of carbon and nitrogen fluxes in mats of purple sulfur bacteria: Implications for carbon cycling at the surface of coastal sediments. *Frontiers in Microbiology*, **8** (OCT), 1–14. <https://doi.org/10.3389/fmicb.2017.01995>
- Jeffrey, S.W. and Humphrey, G.F. (1975) New spectrophotometric equations for determining chlorophylls a, b, c1 and c2 in higher plants, algae and natural phytoplankton. *Biochimie Und Physiologie Der Pflanzen*, **167**(2), 191–194.
- Klatt, C.G., Liu, Z., Ludwig, M., Ku, M., Jensen, S.I., Bryant, D.A. and Ward, D. M. (2013) Temporal metatranscriptomic patterning in phototrophic Chloroflexi inhabiting a microbial mat in a geothermal spring. *ISME Journal*, **7**(9), 1775–1789. <https://doi.org/10.1038/ismej.2013.52>
- Kourilová, X., Schwarzerová, J., Pernicová, I., Sedlár, K., Mrázová, K., Krzyžánek, V., Nebesárová, J. and Obruca, S. (2021) The first insight into polyhydroxyalkanoates accumulation in multi-extremophilic *Rubrobacter xylanophilus* and *Rubrobacter spartanus*. *Microorganisms*, **9**(909), 1–13. <https://doi.org/10.3390/microorganisms9050909>
- Krause, S., Liebetrau, V., Gorb, S., Sánchez-Román, M., Mckenzie, J.A. and Treude, T. (2012) Microbial nucleation of Mg-rich dolomite in exopolymeric substances under anoxic modern seawater salinity: New insight into an old enigma. *Geology*, **40**(7), 587–590. <https://doi.org/10.1130/G32923.1>
- LaRowe, D.E., Arndt, S., Bradley, J.A., Estes, E.R., Hoarfrost, A., Lang, S.Q., Lloyd, K.G., Mahmoudi, N., Orsi, W.D., Shah Walter, S.R., Steen, A.D. and Zhao, R. (2020) The fate of organic carbon in marine sediments - New insights from recent data and analysis. *Earth-Science Reviews*, **204** (February), 103146. <https://doi.org/10.1016/j.earscirev.2020.103146>
- Leifeld, J., Klein, K. and Wüst-Galley, C. (2020) Soil organic matter stoichiometry as an indicator for peatland degradation. *Scientific Reports*, **10**(1), 1–9. <https://doi.org/10.1038/s41598-020-64275-y>
- Lenk, S., Arnds, J., Zerjatke, K., Musat, N., Amann, R. and Mußmann, M. (2011) Novel groups of Gammaproteobacteria catalyze sulfur oxidation and carbon fixation in coastal, intertidal sediment. *Environmental Microbiology*, **13**(3), 758–774. <https://doi.org/10.1111/j.1462-2920.2010.02380.x>
- Liu, D., Xu, Y., Papineau, D., Yu, N., Fan, Q., Qiu, X. and Wang, H. (2019) Experimental evidence for abiotic formation of low-temperature protodolomite facilitated by clay minerals. *Geochimica et Cosmochimica Acta*, **247**, 83–95. <https://doi.org/10.1016/j.gca.2018.12.036>
- Mandal, A., Dutta, A., Das, R. and Mukherjee, J. (2021) Role of intertidal microbial communities in carbon dioxide sequestration and pollutant removal: A review. *Marine Pollution Bulletin*, **170** (December 2020), 112626. <https://doi.org/10.1016/j.marpolbul.2021.112626>
- Mazière, C., Bodo, M., Perdrau, M.A., Cravo-Laureau, C., Duran, R., Dupuy, C. and Hubas, C. (2022) Climate change influences chlorophylls and bacteriochlorophylls metabolism in hypersaline microbial mat. *Science of the Total Environment*, **802**, 149787. <https://doi.org/10.1016/j.scitotenv.2021.149787>
- Mukherji, S., Ghosh, A., Bhattacharyya, C., Mallick, I., Bhattacharyya, A., Mitra, S. and Ghosh, A. (2020) Molecular and culture-based surveys of metabolically active hydrocarbon-degrading archaeal communities in Sundarban mangrove sediments. *Ecotoxicology and Environmental Safety*, **195** (March), 110481. <https://doi.org/10.1016/j.ecoenv.2020.110481>
- Murdock, J.N. (2016) Detecting carbon uptake and cellular allocation by individual algae in multispecies assemblages. *Limnology and Oceanography: Methods*, **14**(2), 124–137. <https://doi.org/10.1002/lom3.10078>
- Patton, C.J. and Kryskalla, J.R. (2003) *Methods of Analysis by the U.S.G.ological Survey National Water Quality Laboratory: Evaluation of Alkaline Persulfate Digestion as an Alternative to Kjeldahl Digestion for Determination of Total and Dissolved Nitrogen and Phosphorus in Water*. U.S. Department of the Interior, U.S.G.ological Survey.
- Paulo, C., McKenzie, J.A., Raof, B., Bollmann, J., Fulthorpe, R., Strohmenger, C.J. and Dittrich, M. (2020) Organomineralization of proto-dolomite by a phototrophic microbial mat extracellular polymeric substances: Control of crystal size and its implication for carbonate depositional systems. *American Journal of Science*, **320**(1), 72–95. <https://doi.org/10.2475/01.2020.05>
- Perri, E., Tucker, M.E., Slowakiewicz, M., Whitaker, F., Bowen, L. and Perrotta, I.D. (2018) Carbonate and silicate biomineralization in a hypersaline microbial mat (Mesaieed sabkha, Qatar): Roles of bacteria, extracellular polymeric substances and viruses. *Sedimentology*, **65**(4), 1213–1245. <https://doi.org/10.1111/sed.12419>
- Petrash, D.A., Bialik, O.M., Bontognali, T.R. R., Vasconcelos, C., Roberts, J.A., Mckenzie, J.A. and Konhauser, K.O. (2017) Microbially catalyzed dolomite formation: From near-surface to burial. *Earth-Science Reviews*, **171**, 558–582. <https://doi.org/10.1016/j.earscirev.2017.06.015>
- Rivers, J.M. (2023) Warm acidified seawater: a dolomite solution. *Journal of Sedimentary Research*, **93**(3), 187–201. <https://doi.org/10.2110/jsr.2022.087>
- Rivers, J.M., Dalrymple, R.W., Yousif, R., Al-Shaikh, I., Butler, J.D., Warren, C., Skeat, S.L. and Abdel Bari, E.M. M. (2020) Mixed siliciclastic-carbonate-evaporite sedimentation in an arid eolian landscape: The Khor Al Adaid tide-dominated coastal embayment, Qatar. *Sedimentary Geology*, **408**, 105730. <https://doi.org/10.1016/j.sedgeo.2020.105730>
- Ruttenberg, K.C. (1992) Development of a sequential extraction method for different forms of phosphorus in marine sediments. *Limnology and Oceanography*, **37**(7), 1460–1482.
- Saintilan, N., Rogers, K., Mazumder, D. and Woodroffe, C. (2013) Allochthonous and autochthonous contributions to carbon accumulation and carbon store in southeastern Australian coastal wetlands. *Estuarine, Coastal and Shelf Science*, **128**, 84–92. <https://doi.org/10.1016/j.ecss.2013.05.010>
- Santos-Andrade, M., Hatje, V., Arias-Ortiz, A., Patire, V.F. and da Silva, L.A. (2021) Human disturbance drives loss of soil organic matter and changes its stability and sources in mangroves. *Environmental Research*, **202** (March), 111663. <https://doi.org/10.1016/j.envres.2021.111663>
- Sanz-Montero, M.E., Cabestrero, Ó. and Sánchez-Román, M. (2019) Microbial Mg-rich carbonates in an extreme alkaline lake (Las Eras, Central Spain). *Frontiers in Microbiology*, **10** (FEB), 1–15. <https://doi.org/10.3389/fmicb.2019.00148>
- Schile, L.M., Kauffman, J.B., Crooks, S., Fourqurean, J.W., Glavan, J. and Megonigal, J.P. (2017) Limits on carbon sequestration in arid blue carbon ecosystems. *Ecological Applications*, **27**(3), 859–874. <https://doi.org/10.1002/eap.1489>
- Song, J., Hwang, J., Kang, I. and Cho, J.C. (2021) A sulfate-reducing bacterial genus, *Desulfosediminicola* gen. nov., comprising two novel species cultivated from tidal-flat sediments. *Scientific Reports*, **11**(1), 1–13. <https://doi.org/10.1038/s41598-021-99469-5>
- Stuart, R.K., Mayali, X., Lee, J.Z., Craig Everroad, R., Hwang, M., Bebout, B.M., Weber, P.K., Pett-Ridge, J. and Thelen, M.P. (2016) Cyanobacterial reuse of extracellular organic carbon in microbial mats. *ISME Journal*, **10**(5), 1240–1251. <https://doi.org/10.1038/ismej.2015.180>
- Suello, R.H., Hernandez, S.L., Bouillon, S., Belliard, J.P., Dominguez-Granda, L., Van De Broek, M., Rosado Moncayo, A.M., Veliz, J.R., Ramirez, K.P., Govers, G. and Temmerman, S. (2022) Mangrove sediment organic carbon storage and sources in relation to forest age and position along a deltaic salinity gradient. *Biogeosciences*, **19**(5), 1571–1585. <https://doi.org/10.5194/bg-19-1571-2022>
- Tang, D., Liu, X., Xia, Z., Hou, J., Yang, X., Li, P. and Yuan, X. (2023) Sources of organic matter and carbon stocks in two mangrove sediment cores and surface sediment samples from Qinglan Bay, China. *Science of the Total Environment*, **893** (June), 164897. <https://doi.org/10.1016/j.scitotenv.2023.164897>
- Trevathan-Tackett, S.M., Seymour, J.R., Nielsen, D.A., Macreadie, P.I., Jeffries, T.C., Sanderman, J., Baldock, J., Howes, J.M., Steven, A.D. L. and Ralph, P.J. (2017) Sediment anoxia limits microbial-driven seagrass carbon remineralization under warming conditions. *FEMS Microbiology Ecology*, **93**(6), 1–15. <https://doi.org/10.1093/femsec/fix033>
- Van de Broek, M., Vandendriessche, C., Poppelmonde, D., Merckx, R., Temmerman, S. and Govers, G. (2018) Long-term organic carbon sequestration in tidal marsh sediments is dominated by old-aged allochthonous inputs in a macrotidal estuary. *Global Change Biology*, **24**(6), 2498–2512. <https://doi.org/10.1111/cb.14089>

- Van Lith, Y., Warthmann, R., Vasconcelos, C. and McKenzie, J.A. (2003) Sulphate-reducing bacteria induce low-temperature Ca-dolomite and high Mg-calcite formation. *Geobiology*, **1**(1), 71–79. <https://doi.org/10.1046/j.1472-4669.2003.00003.x>
- Vasconcelos, C. and McKenzie, J.A. (1997a) Microbial mediation of modern dolomite precipitation and diagenesis under anoxic conditions (Lagoa Vermelha, Rio de Janeiro, Brazil). *Journal of Sedimentary Research*, **67**(3), 378–390.
- Vasconcelos, C. and McKenzie, J.A. (1997b) Microbial mediation of modern dolomite precipitation and diagenesis under anoxic conditions (Lagoa Vermelha, Rio de Janeiro, Brazil). *Journal of Sedimentary Research*, **67**(3), 378–390. <https://doi.org/10.1306/D4268577-2B26-11D7-8648000102C1865D>
- Vasconcelos, C., Dittrich, M. and McKenzie, J.A. (2014) Evidence of microbiocoenosis in the formation of laminae in modern stromatolites. *Facies*, **60**, 3–13. <https://doi.org/10.1007/s10347-013-0371-3>
- Wainwright, B.J., Millar, T., Bowen, L., Semon, L., Hickman, K.J. E., Lee, J.N., Yeo, Z.Y. and Zahn, G. (2023) The core mangrove microbiome reveals shared taxa potentially involved in nutrient cycling and promoting host survival. *Environmental Microbiome*, **18**(47), 1–12. <https://doi.org/10.1186/s40793-023-00499-5>
- Wang, B., Liu, N., Yang, M., Wang, L., Liang, X. and Liu, C.Q. (2021) Co-occurrence of planktonic bacteria and archaea affects their biogeographic patterns in China's coastal wetlands. *Environmental Microbiomes*, **16**(1), 1–12. <https://doi.org/10.1186/s40793-021-00388-9>
- Wasmund, K., Mußmann, M. and Loy, A. (2017) The life sulfuric: microbial ecology of sulfur cycling in marine sediments. *Environmental Microbiology Reports*, **9**(4), 323–344. <https://doi.org/10.1111/1758-2229.12538>
- Wright, D.T. and Wacey, D. (2005). Precipitation of dolomite using sulphate-reducing bacteria from the Coorong Region, South Australia: Significance and implications. *Sedimentology*, **52**(5), 987–1008. <https://doi.org/10.1111/j.1365-3091.2005.00732.x>
- Wunderlin, T., Junier, T., Roussel-Delif, L., Jeanneret, N. and Junier, P. (2014) Endospore-enriched sequencing approach reveals unprecedented diversity of Firmicutes in sediments. *Environmental Microbiology Reports*, **6**(6), 631–639. <https://doi.org/10.1111/1758-2229.12179>
- Yang, M., Liu, N., Wang, B., Li, Y., Li, J. and Liu, C.Q. (2022) Archaeal contribution to carbon-functional composition and abundance in China's coastal wetlands: Not to be underestimated. *Frontiers in Microbiology*, **13** (November), 1–11. <https://doi.org/10.3389/fmicb.2022.1013408>
- Yu, L., Daniels, L.M., Mulders, J.J.P.A., Saldi, G.D., Harrison, A.L., Liu, L. and Oelkers, E.H. (2019) An experimental study of gypsum dissolution coupled to CaCO₃ precipitation and its application to carbon storage. *Chemical Geology*, **525** (May), 447–461. <https://doi.org/10.1016/j.chemgeo.2019.08.005>
- Zhang, S. (2020) The relationship between organoclastic sulfate reduction and carbonate precipitation/dissolution in marine sediments. *Marine Geology*, **428** (November 2019), 106284. <https://doi.org/10.1016/j.margeo.2020.106284>
- Zhang, X., Zhang, C., Liu, Y., Zhang, R. and Li, M. (2023) Non-negligible roles of archaea in coastal carbon biogeochemical cycling. *Trends in Microbiology*, **31** (6), 586–600. <https://doi.org/10.1016/j.tim.2022.11.008>
- Zhao, R., Dong, X., Liu, Q., Xu, M. and Zhao, Y. (2023) Distribution, sources and influencing factors of organic carbon in the surface sediments of the coastal tidal flats in Jiangsu Province. *Frontiers in Marine Science*, **10** (July), 1–13. <https://doi.org/10.3389/fmars.2023.1220923>